

Design and Analysis for a CubeSat Mission

A Major Qualifying Project Report
Submitted to the Faculty of
WORCESTER POLYTECHNIC INSTITUTE
in Partial Fulfilment of the Requirements for the
Degree of Bachelor of Science
In Aerospace Engineering

By



Jeremy Gagnon



Christopher Ritter



Drake Tierney

March 7, 2022

Approved by:

Michael A. Demetriou, Advisor
Professor, Aerospace Engineering Program
Worcester Polytechnic Institute

ABSTRACT

This project supports the design of a 6U CubeSat utilizing the NASA-designed miniature Ion Neutral Mass Spectrometer (mini-INMS) and Gridded Retarding Ion Drift Sensor (GRIDS) to measure the composition of the ionosphere's F layer. The CubeSat will operate in a semi-Sun-synchronous elliptical orbit with a perigee of 180 km and apogee of 600 km. This report covers the attitude determination and control, telemetry and communications, and the command and data handling subsystems of this mission, in addition to the mission payload. Attitude dynamics modeling was performed using Systems Tool Kit (STK) along with MATLAB's Simulink software. Attitude control required actuation via magnetorquers and reaction wheels, guided by an on-board computer. Telecommunications analysis was performed using STK.

"Certain materials are included under the fair use exemption of the U.S. Copyright Law and have been prepared according to the fair use guidelines and are restricted from further use."

ACKNOWLEDGEMENTS

We would like to thank the Professors Demetriou, Taillefer and Gatsonis for their help and support throughout the entirety of this project

AUTHORSHIP PAGE

Section	Author
<i>Introduction</i>	All
<i>Payload</i>	All
<i>Attitude Determination and Control</i>	
3.1-3.4, 3.5.1, 3.5.4, 3.6.1, 3.6.3, 3.6.4	JG
3.5.2, 3.5.2, 3.6.2	CR
<i>Telemetry and Communications</i>	DT
<i>Command and Data Handling</i>	CR
<i>Conclusion and Recommendations</i>	JG

Table of Contents

ABSTRACT.....	iii
ACKNOWLEDGEMENTS.....	iv
AUTHORSHIP PAGE.....	v
TABLE OF FIGURES.....	viii
TABLE OF TABLES.....	ix
1. Introduction.....	10
1.1. Background and Literature review.....	11
1.2. Societal Impacts Report.....	13
1.3. Environmental Impacts Report.....	13
1.4. Economic Impact Report.....	14
1.5. Project Goals.....	14
1.6. Project Design Requirements, Constraints and Other Considerations.....	15
1.6.1. Subsystem Requirements.....	15
1.6.2. Satellite Dispenser Selection and Constraints.....	16
1.6.3. Satellite Launch Vehicle Requirements and Constraints.....	18
2. Payload.....	19
2.1. Mini-Ion Neutral Mass Spectrometer (INMS).....	19
2.2. Gridded Retarding Ion Drift Sensor (GRIDS).....	23
3. Attitude Determination and Control.....	26
3.1. Overview.....	26
3.2. Mission Requirements.....	26
3.3. Component Selection.....	27
3.3.1. Actuator Sizing and Selection.....	28
3.3.2. Sensor Selection.....	32
3.3.3. Gyroscope.....	32
3.3.4. Magnetometer.....	33
3.3.5. Sun Sensors.....	34
3.3.6. Accelerometer.....	37
3.3.7. GPS.....	38
3.4. Detumbling.....	38
3.5. Attitude Determination.....	43
3.5.1. TRIAD.....	43
3.5.2. Wahba's Question.....	46
3.5.3. Davenport's q-Method.....	48
3.5.4. QUEST.....	49
3.6. Attitude Control.....	51
3.6.1. Reaction Wheel Sizing.....	51
3.6.2. Extended Kalman Filter.....	53
3.6.3. STK.....	59
3.6.4. Simulink.....	61
4. Telemetry and Communications.....	63
4.1. Overview.....	63
4.2. Component Selection.....	65
4.2.1. Ground Stations.....	66
4.2.2. Transceiver.....	67

4.2.3. Antenna	67
4.3. Results.....	68
4.4. WPI Ground Station Set-Up	69
5. Command and Data Handling.....	71
5.1. Overview.....	71
5.2. Component Selection	71
5.2.1. Previous On-Board Computers	71
5.2.2. Chosen On-Board Computer.....	72
6. Conclusion and recommendations	73
REFERENCES	75
APPENDIX A: Kryten M3 Tech Sheet	77

TABLE OF FIGURES

Figure 1: Rail CubeSat Dispenser.....	17
Figure 2: Tabs CubeSat Dispenser.....	18
Figure 3: Gated Time-of-Flight (TOF) Apparatus [2]	21
Figure 4:Counts of detected masses according to their TOF [2]	21
Figure 5:The Mini-INMS species collection system [2].....	22
Figure 6:Initial Ion Measurements from the INMS aboard NASA Dellingr [4]	23
Figure 7: The GRIDS apparatus [X].....	25
Figure 8: Grids within the GRIDS system [X]	25
Figure 9: iMTQ Magnetorquer Board.....	29
Figure 10: RWP050 Reaction Wheel.....	31
Figure 11: ADXRS453 Gyroscope	33
Figure 12: XEN1210 Magnetometer	34
Figure 13: NFSS-411 Fine Sun Sensor	36
Figure 14: Hyperion SS200 Coarse Sun Sensor	36
Figure 15: STM IIS3DHHHC Accelerometer	37
Figure 16: FBD of Appleton’s Geomagnetic Attitude Control	39
Figure 17:Attitude Configuration of Appleton	40
Figure 18:Appleton’s STK Attitude Simulation.....	61
Figure 19: Detumble Simulation Diagram.....	63
Figure 20: Maintenance Simulation Diagram.....	63
Figure 21: Kryten-M3	72

TABLE OF TABLES

Table 1: Parameters and performance of the Mini-INMS.	20
Table 2: Parameters and performance of the Mini-INMS [2], [3].....	24
Table 3: iMTQ Specifications.....	30
Table 4: RWP050 Specifications.....	32
Table 5: ADXRS453 Specifications.....	33
Table 6: XEN1210 Specifications.....	34
Table 7: NFSS-411 Specifications.....	36
Table 8: SS200 Specifications.....	37
Table 9: IIS3DHHHC Specifications.....	38
Table 10: Kyten-M3 Plus GPS Specifications.....	38
Table 11: Radio Frequencies.....	65
Table 12: Ground Station Access Times.....	66
Table 13: Transceiver Data.....	67
Table 14: Antenna Data.....	68
Table 15: File Size Per Data Collection Time.....	68
Table 16: Previous On-Board Computers.....	71

1. INTRODUCTION

Since the first artificial earth satellite launch in 1957, hundreds of satellites have been launched for a variety of scientific endeavors. Many of these sophisticated spacecrafts require significant resources unattainable by most non-governmental organizations. In order to make scientific missions more accessible to those without these resources, recent advances have been made to develop compact, low cost, and low power spacecraft capable of carrying scientific payloads. One such development, the CubeSat, was created in 1999 by Stanford University's Space Systems Development Lab in conjunction with students at California Polytechnic State University, San Luis Obispo. This spacecraft utilizes a standard 1U unit (1000 cm^3) structure with a mass of up to 1.33 kg. Modular in nature, this standard unit can be combined in order to build larger configurations, such as the 6U model used for the Appleton CubeSat mission. This allows for expanded capabilities and large payloads for scientific missions. Initially developed solely for educational purposes, current advancements have allowed this spacecraft design to conduct missions with high scientific and commercial returns.

The goal of this Major Qualifying Project (MQP) is to develop the conceptual design of the Appleton CubeSat, carrying a Miniaturized Ion Neutral Spectrometer (INMS) and a Gridded Retarding Ion Drift Sensor (GRIDS), as well as to utilize a Helmholtz Cage to recreate the magnetic environment the spacecraft shall experience during orbit. Appleton is a 6U CubeSat that will enter a polar sun-synchronous extreme low earth orbit (eLEO) with a perigee of 180 kilometers in order to gather data regarding neutral and ionized particle densities in the ionosphere. This MQP builds off the research done in several past MQP's, primarily the 2019 Systems Engineering Group's NIMS ELEO Atmospheric Observer and 2020 Systems

Engineering Group's Magnetospheric near Sun-synchronous Tumbling Attitude Research Satellite.

Appleton is to be deployed from SpaceX's Falcon 9 launch vehicle via the SmallSat Rideshare Program at an altitude of approximately 600 kilometers and an inclination of 97.34 degrees. It will then initiate two separate finite burn transfers in order to achieve a final sun-synchronous orbit with a perigee of 180 kilometers and an apogee of 800 kilometers. Once in the final scientific orbit, data collection will occur for the duration of the mission until deorbit. The Systems Engineering Group for this MQP is comprised of Mechanical, Propulsion, Power, Payload, Attitude Determination and Control (ADCS), Telemetry and Communication, Command and Data Handling, Thermal, and Space Environment subsystems. The responsibility of developing and testing the Helmholtz Cage for ADCS analysis will be shared by each subsystem.

1.1. Background and Literature review

Cube Satellites, also known as CubeSats, are small orbital spacecraft used for a variety of scientific and military missions in Earth's orbit. CubeSats are dimensioned into 10 X 10 X 10 cm units, denoted 'U', and are often composed of 1, 2, 3, 6, or 12 of these cubic units. The term 'Nano-satellite' refers to any satellite weighing between 1 and 10 kg and is a specification of CubeSats. CubeSats were developed by two professors from California Polytechnic Institute and Stanford University in the late 1990s and have seen significant growth ever since. CubeSats are typically sent into orbit via the upper stage of launch vehicles as auxiliary payloads.

Initially designed as low-cost test vehicles for satellite capabilities and design, and slowly developed into modern day space applications, CubeSats are being used for a wide variety of research and communications missions and have undergone many design innovations. Typically, CubeSats operate in lower Earth orbit, which makes them ideal for communications and atmospheric research purposes. In the past few years, NASA's CubeSat Launch Initiative (CSLI) has been working to provide more opportunities to send satellites as secondary payloads on commercial or NGO launch craft.

Cube satellites (CubeSats) are miniature satellites used for space research and technology development. They are a particular class of nanosatellites that was developed by California Polytechnic State University and Stanford University in 1999 in order to promote the design, manufacture, and testing of satellite technology in low Earth orbit [1]. CubeSats are comprised of multiple 10 cm by 10 cm by 10 cm units, referred to as 'U's. Layouts can vary greatly, but the most common form factors are 1U and 3U [1]. In recent years, larger CubeSats have been developed to increase available space for mission payloads. Typically, CubeSats are deployed by a launch mechanism attached to the upper stage of a launch vehicle and offer an easy way to deploy CubeSats into Earth orbit. The CubeSat concept began as a plan to provide scientific and military laboratories a tool to grow their operations in space [2]. In recent years, the CubeSat has become a unique tool in the scientific community. NASA's CubeSat Launch Initiative (CSLI) provides opportunities to launch CubeSats aboard larger launch vehicles as secondary payloads [3]. CubeSats are currently in an era of rapid growth; it is estimated that the global CubeSat market was valued at \$152 million in 2018, and is projected to rise to nearly \$375 million in coming years [4].

1.2. Societal Impacts Report

The CubeSat industry is one of the fastest growing markets in the space sector. Due to the low cost of building CubeSats and increased accessibility to launch vehicles like SpaceX's Falcon 9 workhorse, sending private space missions into LEO is becoming more possible for universities and research institutions previously restricted from establishing projects in space by financial constraints. This increased accessibility to space research will prove revolutionary to our societies' relationship with space and scientific education as humanity prepares to make its first interplanetary leap to Mars.

Focusing on Appleton's ionospheric mission specifically, there are numerous benefits to learning more about the behavior of Earth's ionosphere. To start, most of the satellites orbiting the Earth exist in or pass through the ionosphere during their lifetimes, making it an important region to study for the success and growth of future satellite programs. Beyond its importance to satellite science, the ionosphere can distort radio or GPS signals, making a better understanding of this region crucial to maintaining good communication across the globe. Finally, space weather and solar activity can be measured more effectively in the ionosphere. The ability to better understand and anticipate space weather activity such as solar flares is vital to the well-being of society, making the ionosphere a critical area of space research.

1.3. Environmental Impacts Report

Most spacecraft require significant resources unattainable by most non-governmental organizations. CubeSats were developed with accessibility in mind, enabling a host of educational, commercial, and scientific applications while reducing cost and resource demand.

While CubeSats still use a substantial amount of resources the cost-benefit payoff is much higher, the overall impact of CubeSat programs is ever-growing. From helping to predict storm strengths and the direction of forest fires to testing new technology in a variety of environments, CubeSats present an array of diverse benefits and opportunities for environmental research and observation.

1.4. Economic Impact Report

Due to the relatively low cost of CubeSats there are several economic benefits that come from their production and use. In terms of large corporations and research firms, CubeSats offer the ability to cheaply test new scientific appliances. In terms of smaller businesses, it is possible to get in the satellite business due to the low cost of CubeSats and the low size of CubeSats allow for them to piggyback on larger launches. These economic benefits allow for the continued development of CubeSats and spacecraft in general as it is possible to test new scientific instruments with minimal risk.

1.5. Project Goals

The overall goal of this MQP is to continue the series of CubeSat research projects done as part of the MQP program at WPI.

The primary goal of the project is to design a CubeSat for a particular scientific mission. This year the satellite will follow a polar sun-synchronous orbit with an apogee of 800 km and a perigee of 180 km. The mission is to study the composition of the F1 and F2 ionosphere layers (altitude of 250-400 km) using two onboard payload sensors: GRIDS and mini-INMS capable of

measuring the situ density, temperature, relative concentration of ions and their velocity. The ionosphere modifies radio signals used for communication and navigation; it is important to study the ionosphere to reduce errors experienced due to its effects on radio waves [1]. To complete the primary goal the team split the design into eight subsystems with each team member responsible for one: mechanical design and analysis, attitude determination and control, telemetry and communications, command and data handling, thermal, power, propulsion, space environment and payload. The role of each subsystem in the CubeSat design is discussed at the beginning of the respective sections.

The second goal of the project is to continue previous MQP work on building and testing the Helmholtz cage. A Helmholtz cage is used for ground testing of the ADCS. It can generate a dynamic magnetic field that is meant to replicate the Earth's magnetic field. During the mission the onboard ADCS is affected by the Earth's magnetosphere, therefore, it is important to test verify it will be functional under such conditions.

1.6. Project Design Requirements, Constraints and Other Considerations

1.6.1. Subsystem Requirements

Payload Requirements:

- The spacecraft shall be capable of assessing the local composition and state of the ionosphere.

ADCS Requirements:

- The system shall maintain 3-axes of attitude knowledge better than 1 degree from apogee to perigee.

- The satellite will successfully detumble, meaning it shall obtain negligible rotational velocity-less than 10 degrees per second-about at least two axes.
- The spacecraft shall achieve sufficient torque authority to overcome predicted disturbance torques from atmospheric drag, magnetic field influence, and thrust vector misalignment.
- The spacecraft shall use this torque authority to maintain a steady orientation of +/- 5 degrees off its pre-modeled nadir pointing attitude vector

Telemetry requirements:

- The spacecraft shall have adequate data rate for command uplink over the orbital period.
- The spacecraft shall have adequate data rate to downlink science data collected and stored.

Command and data handling.

- The spacecraft shall have the computational capability for closed loop ADC.
- The spacecraft shall have data capacity for science data.

1.6.2. Satellite Dispenser Selection and Constraints

Prior to mission the CubeSat is contained within a satellite dispenser that attaches to the launch vehicle. The dispenser has a spring-loaded door on one side that activates and dispenses the satellite at the desired altitude (Puig-Suari and Nugent, 2015). There are two types of CubeSat dispensers. Both dispense the vehicle using a spring-loaded pushing plate, the difference is how the satellite is secured within the dispenser.

First method, used in Tyvak and Innovative Solutions In Space (ISIS) dispensers, is four rails at each corner of the satellite (Figure 1). The rail dispenser provides extra insulation between the payload and the outer part of the dispenser, the insulators are located in the 0.5 mm gap between the rails and the outer wall. In this configuration the payload might vibrate making it impossible to model accurately.

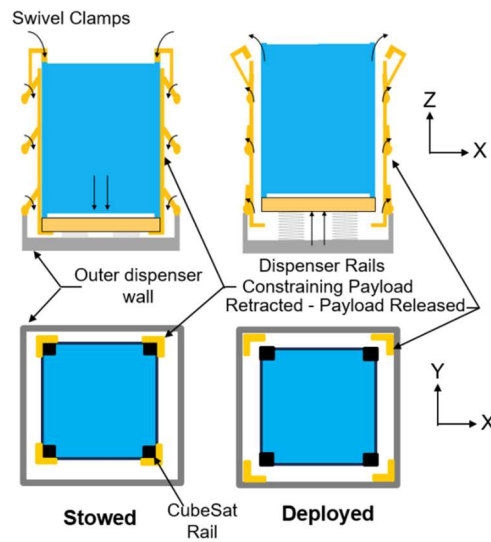


Figure 1: Rail CubeSat Dispenser

The second method, used in Planetary Systems Corporation dispensers, is using two thinner rails or tabs, that are clamped to the dispenser (Figure 1). Tabs provide a secure connection between the payload and the dispenser allowing for accurate modelling of the systems responses to vibrations and loading. The MQP project is focused on the design phase of the satellite mission, therefore it is important to have accurate predictions using software. For our project we chose the Canisterized Satellite Dispenser (CSD) with tabs. In addition, payload specifications for the Planetary Systems Corporation (PSC) dispenser were available online, which made it easier to follow requirements when modelling.

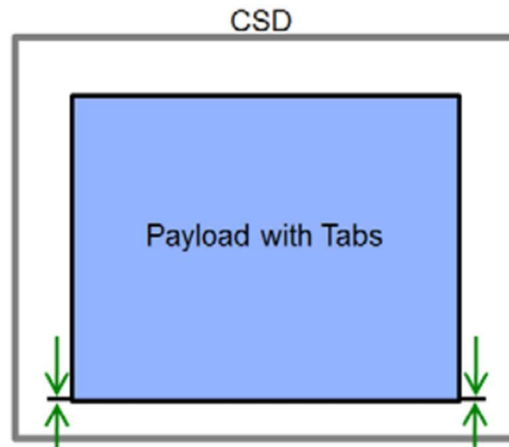


Figure 2: Tabs CubeSat Dispenser

Once the satellite dispenser was chosen several constraints were applied to the design. CSD is a standard unit that is manufactured by PSC, therefore, the payload must follow the requirements provided in the Payload Specification (Planetary Systems Corporation, 2018). There is around 389.56 cm^3 volume that the CubeSat can occupy, there is a 9.1 kg maximum mass limit, constraints on the location of the center of mass and the maximum tab loading cannot exceed 3559 N. Further break down of these requirements and their effects on the design can be found in section 3 Mechanical Design.

1.6.3. Satellite Launch Vehicle Requirements and Constraints

There have been 19 missions where CSD was used to dispense CubeSatellites, from these missions we can identify several launch vehicles that are proven to be compatible with this system: Electron (6 missions), Falcon 9 (5 missions), Atlas 5 (3 missions), SPARK (1 mission), Minotaur IV (1 mission), PSLV-CA (1 mission), LauncherOne (1 mission) and Antares (1 mission). Due to the requirements of the mission orbit, as well as the availability and accessibility of information, SpaceX's Falcon 9 rocket was chosen as the primary launch vehicle.

Appleton will utilize the SmallSat Rideshare program and be attached to a mechanical interface rig.

The Falcon 9 rocket will eject the CubeSat into an initial parking orbit with an apogee and perigee of approximately 500 to 600 kilometers. The orbit will share the inclination of the final orbit, with a value of 97.34 degrees. This will allow Appleton to be sun-synchronous, meaning that the spacecraft will process with the same period as Earth's solar orbit. This is optimal as the CubeSat will need to be sun-facing in order to optimize power generation.

2. PAYLOAD

The goal of this scientific mission is to interrogate the ionosphere across the F1 and F2 layers to collect data regarding the local composition and state of the ionic and neutral species. To accomplish this, two separate devices, the Mini-Ion Neutral Mass Spectrometer (Mini-INMS) and Gridded Retarding Ion Drift Sensor (GRIDS) were selected. Both instruments, when used in tandem, provide measurements of the densities of neutral and ionized species in the ionosphere, as well as relative ion concentrations, temperatures, and velocity vectors (component normal to instrument face).

2.1. Mini-Ion Neutral Mass Spectrometer (INMS)

NASA Goddard's Mini-INMS can provide in situ density measurements of ion and neutral species in the ionosphere. Specifically, it can measure densities of the species shown in Table 1.

Parameter	Performance
Ion Species	H ⁺ , He ⁺ , N ⁺ , O ⁺ , NO ⁺ , O ₂ ⁺
Ion Range	10 ³ cm ⁻³ to 10 ⁷ cm ⁻³
Neutral Species	H, He, N, O, N ₂ , O ₂
Neutral Range	10 ⁵ cm ⁻³ to 10 ⁹ cm ⁻³
Volume	1.3 U
Mass	960 g
Power	1.8 W
Cadence	1 s
Data Rate	13.1 kbit/s
Operating Temperature	-10 to 50 °C
FOV	±20° x ±10° around ram

Table 1: Parameters and performance of the Mini-INMS.

The Mini-INMS measures these densities using a gated time-of-flight (TOF) instrument as shown in Figure 1. Both the neutral and ion apertures use this instrument to measure the mass of each species according to their TOF.

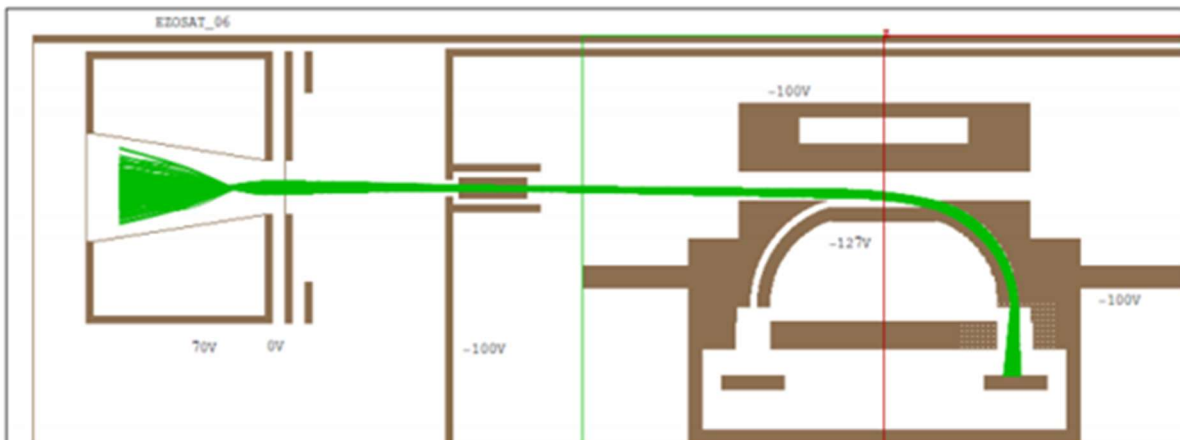


Figure 3: Gated Time-of-Flight (TOF) Apparatus [2]

On the ion side, particles enter the aperture and receive a pre-acceleration voltage which gives all ions essentially the same energy. While the energy of incoming ions will vary, the voltage applied is orders of magnitude greater, thereby negating this difference. With all ions having the same kinetic energy their velocity into the instrument will be solely dependent on the particle mass; heavier ions will travel more slowly than lighter ions. The faster moving ions will have a lower time of flight (TOF) than heavier ions; by ordering ions in their velocity according to their mass a TOF model can be created for the collection period, as shown in Figure 2.

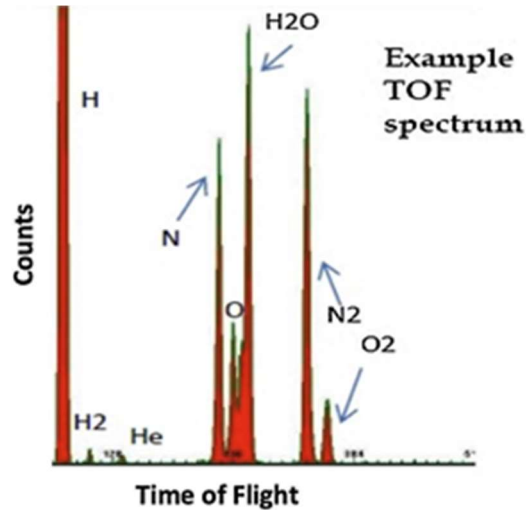


Figure 4: Counts of detected masses according to their TOF [2]

Similarly, on the neutral side, particles are also given an initial pre-acceleration voltage to use the same TOF methods as on the ion side. The main difference between the two is that the neutral side also contains an ion repellant at the aperture to only allow neutral particles entry. In this way the densities of both the ionized and neutral species can be measured. The entire apparatus is shown in Figure 3.

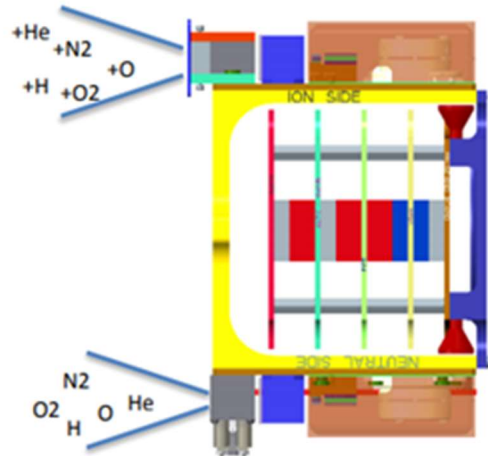


Figure 5: The Mini-INMS species collection system [2]

The functionality of the INMS has been proven in multiple missions including ExoCube, Dellinger, and petitSat. The ExoCube, flown in 2015, was the first flight of the Mini-INMS. However, due to inadequate antenna deployment on the CubeSat the data received was less than desired. The instrument functioned well and was able to send TOF spectrums that aligned with those predicted, such as the sample shown in Figure 2, but ultimately communication with the CubeSat was lost [2]. Unfortunate circumstances also occurred with the NASA Dellinger spacecraft, launched in 2017. The CubeSat was accidentally powered before deployment resulting in a dead battery from the start of the mission [4]. While the CubeSat was able to recover using its solar panels. After the completion of outgassing the remaining particles left in the INMS from Earth's atmosphere the satellite was able to successfully activate and record data from the ion side of the INMS as shown in Figure 4. Data from the neutral side of the INMS has not been able to be demonstrated by this mission.

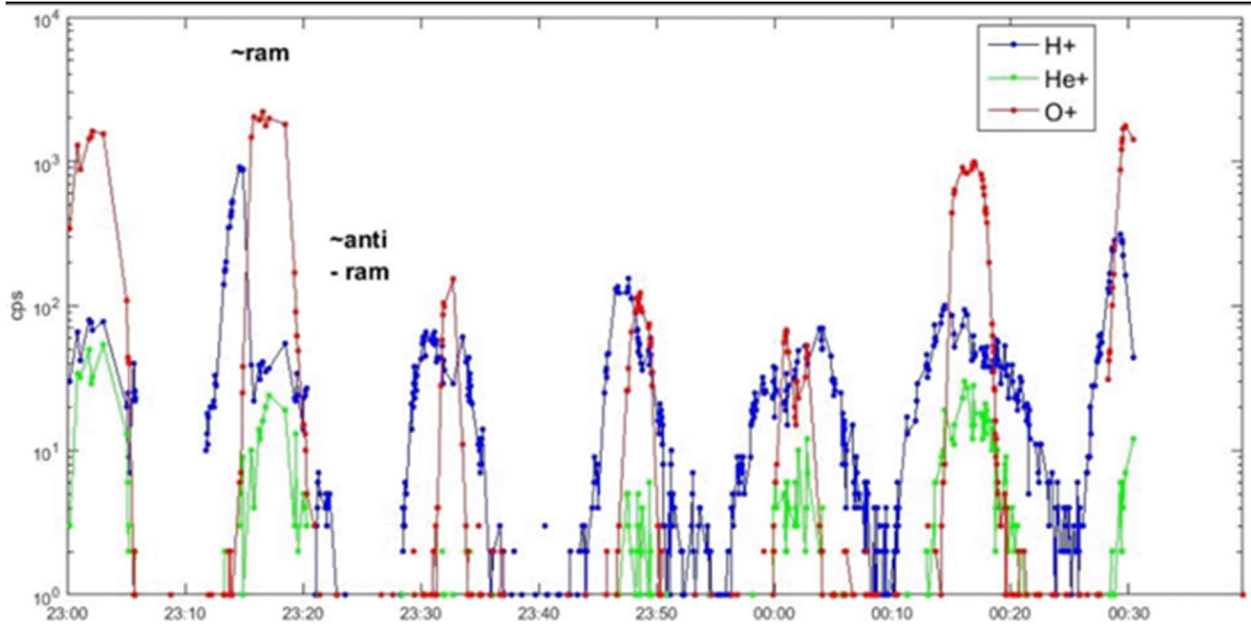


Figure 6: Initial Ion Measurements from the INMS aboard NASA Dellingr [4]

2.2. Gridded Retarding Ion Drift Sensor (GRIDS)

The GRIDS system can provide in situ ion density, temperature, relative concentration of heavy to light ions, and the component of the velocity vector normal to the instrument face. Specifically, it can measure the parameters shown in Table 2.

Parameter	Performance
Velocity Range (Accuracy)	-1500 m/s to 1500 m/s (± 10 m/s)
Ion Species	H ⁺ , He ⁺ , O ⁺
Ion Density Range (Accuracy)	$5 \times 10^3 \text{ cm}^{-3}$ to $5 \times 10^7 \text{ cm}^{-3}$ (500 cm^{-3} or 2%)
Ion Temperature Range (Accuracy)	0 K to 3000 K (10 K or 5%)
Ion Composition Range (Accuracy)	0 to 1 (0.02)
Volume	0.75 U

Mass	500 g
Power	0.5 W
Cadence	0.5 Hz
Data Rate	533 bit/s
Operating Temperature	-20 to 80 °C

Table 2: Parameters and performance of the Mini-INMS [2], [3]

The GRIDS device is made of a series of biased and grounded grids located behind a RAM facing aperture. These grids are supplied with a retarding voltage to act as ion-energy filters [4]. At the back of the instrument there are ion collectors which detect currents produced from ion impacts. By varying the retarding voltage in the aperture grids the ion species can be selectively allowed to pass through and into the collectors. Current from ions impacting the collector is used to calculate total ion flux as a function of retarding voltage [4]. From this calculation the ion density, temperature, relative concentration of heavy to light ions, and the component of the velocity vector normal to the instrument face can be derived. The grids sensor and the breakdown of its internal grids are shown in Figures 5 and 6.

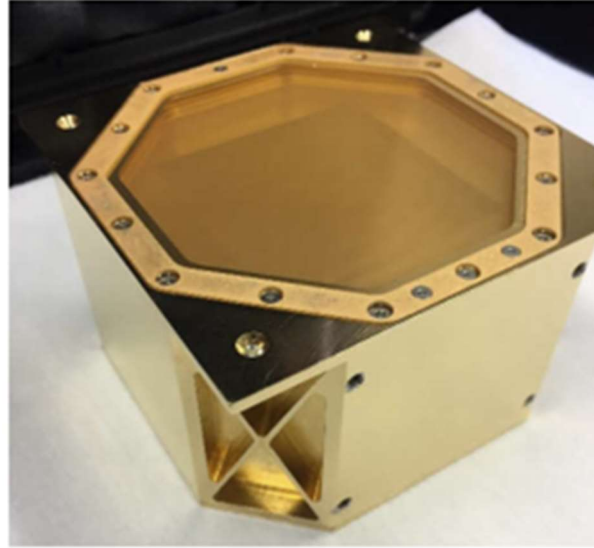


Figure 7: The GRIDS apparatus [X]

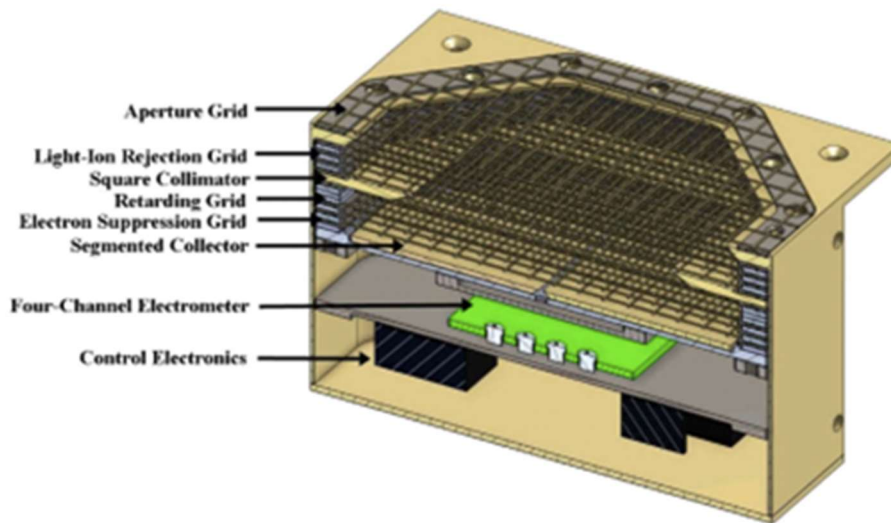


Figure 8: Grids within the GRIDS system [X]

The GRIDS system and the Mini-INMS were both selected for the petitSat mission, deploying from the ISS in 2021, this mission will help determine the link between plasma enhancements and medium-sized traveling ionospheric disturbances (MSTIDs).

3. ATTITUDE DETERMINATION AND CONTROL

3.1. Overview

The spacecraft's Attitude Determination and Control system (ADCS) is responsible for properly orienting the spacecraft throughout orbit so that it can fulfill all necessary mission requirements. This requires the ADCS to accomplish three central objectives over the course of the mission:

1. Detumbling
2. Attitude determination
3. Attitude maintenance

The ADCS satisfies these objectives via a closed-loop control system that connects various sensors with electromagnetic and inertial actuators.

3.2. Mission Requirements

In completing the central objectives of the Attitude Determination and Control subsystem, the Appleton satellite must be stabilized and maintain a steady orientation of +/- 5 degrees off its pre-modeled nadir pointing attitude vector.

Upon release from the launch vehicle, Appleton will be imparted with significant rotational motion in all three axes as it enters the space environment. Before proceeding with the additional mission objectives, Appleton will need to reduce this rotational motion to a point where steady attitude determination and maintenance are possible through a process known as

detumbling. To successfully be considered detumbled, Appleton must achieve a rotational velocity of less than 10 degrees per second about at least two of its axes.

Once the satellite has detumbled, it will be required to counter any disturbance torque to maintain its attitude within the pre-determined margin of error. This disturbance torque can come from a variety of sources, including atmospheric drag, gravity gradient drags, solar wind, and interactions between the Earth's magnetosphere and onboard components. The most critical of these disturbance torque considerations will be the aerodynamic drag due to interactions with the Earth's atmosphere. Due to Appleton's low elliptical orbit, the spacecraft will be vulnerable to atmospheric drag repeatedly over the course of the mission. Additionally, atmospheric drag induces disturbance torque exponentially if left uncorrected, making this an important consideration when designing Appleton's attitude maintenance system.

3.3. Component Selection

Appleton's ADCS system is composed of a suite of onboard sensors and actuators which work to obtain spacecraft attitude data and perform attitude corrections, respectively. The CubeSat market has seen rapid growth over the past decade which has generated a diverse selection of small satellite components for independent projects like ours. When selecting components for Appleton's ADCS system, several variables were considered and weighed against one another to find the best fit as dictated by our mission requirements.

The flight heritage, mass, and power requirements were considered for both sensors and actuators alike. More specific variables like data resolution and torque output were also considered for sensors and actuators, respectively. Further considerations included complexity of implementation in our spacecraft's design and relative cost of components. While all

components are essential for proper attitude control, variables were weighted differently depending on the component and its contribution to the mission. The suite of sensors required to provide Appleton with continuous attitude knowledge includes sun sensors (both coarse and fine), a magnetometer, a gyroscope, GPS, and an accelerometer. The actuators needed to maintain attitude control of our satellite were magnetorquers and reaction wheels, set along all three rotational axes. A closed loop control system which will link the determination and control sides of this system will be supported by an on-board computer covered in the Command and Data Handling section of this report.

3.3.1. Actuator Sizing and Selection

For Appleton to successfully meet its mission requirements for attitude control, it must use actuators to reduce its initial angular velocity and then counteract any disturbance torques imparted by the environment. A common solution to the CubeSat attitude control problem is the combined use of electromagnetic and inertial actuators which act as the primary attitude control over different legs of the mission and can also be used as fail-safes in the case of primary system saturation.

The central considerations when deciding on specific actuator technology came down to the ability of the actuator to provide sufficient control torque to satellite, while remaining power and mass efficient. This sufficient torque was calculated separately for the detumble and attitude maintenance sections of our mission and can be found later in this report.

The first mission requirement, or the act of detumbling the satellite, will be accomplished by magnetorquers. Magnetorquers function as attitude actuators by running an electric current through a rod of coiled wire, creating an electromagnetic dipole. This dipole interacts with the Earth's magnetosphere, generating a torque which the satellite can use to slow rotational motion.

$$\vec{L} = \vec{m} \times \vec{B} \quad (1)$$

Traditionally, magnetorquers are configured in sets of three, with one dipole running along each of the spacecraft's axes. Many magnetorquers on the market today are sold as pre-built three-dimensional attitude control boards for easier integration into satellite systems. For the purposes of our project, we wanted to choose a magnetorquer board which was packaged and preprogrammed with a magnetometer. This would enable us to trust our magnetometer readings while avoiding the computationally heavy task of filtering out noise generated by our actuators or adding to Appleton's mechanical complexity by deploying the magnetometer on a boom. The magnetorquer board we decided on was the ISIS iMTQ, which was heavily considered in last year's project. The iMTQ Magnetorquer Board has all around good marks in flight heritage, dipole magnitude, and low mass/voltage usage.

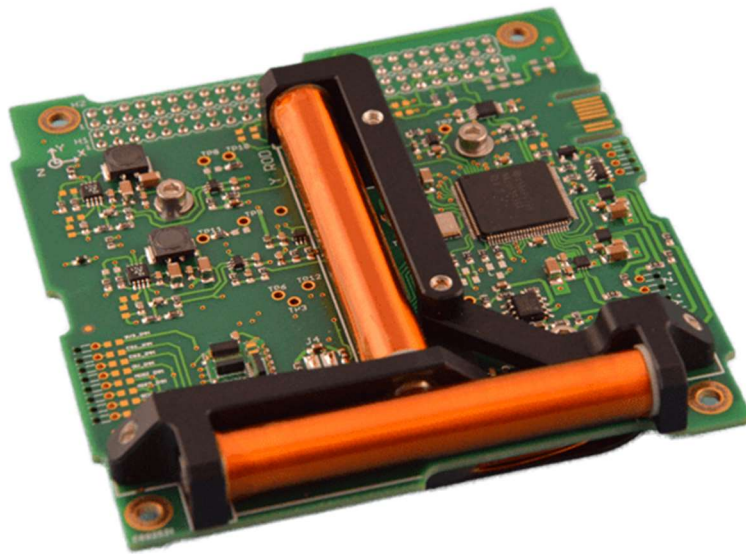


Figure 9: iMTQ Magnetorquer Board

Parameter	Value
Mass	0.2 Am ²
Power Consumption	175 mW - <1.2 W
Mass	196 g
Operating Temperature	-40 C to 70 C
Voltage	5 V
Dimensions	95.9 X 90.1 X 17 mm

Table 3: iMTQ Specifications

For the second phase of the ADCS mission, reaction wheels will be used to maintain satellite attitude and accomplish any pointing maneuvers required by the propulsion subsystem. Reaction wheels provide torque to the spacecraft via the law of conservation of momentum. When active, reactions wheels use a brushless DC motor to spin a weighted flywheel, generating angular momentum. By changing the speed at which the flywheel rotates, reaction wheels can generate an equal and opposite torque since the total momentum in the spacecraft body will always remain the same. Reaction wheels make ideal attitude control actuators for small satellites because they are electrically powered and therefore unburdened by the fuel storage requirements of chemical attitude control thrusters. Reaction wheels also add stability to spacecraft attitude simply by being constantly active and rotating, once again due to the law of conservation of momentum. For the three-dimensional attitude control required by our mission, we will use three reaction wheels -- with one positioned along each axis -- as each wheel can only impart torque along its axis of rotation.

The reaction wheel selected was also chosen by the 2020 project team. The RWP050 can produce a maximum torque of 0.007 Nm, resulting from a generated moment of up to 0.05 Nms about a given axis while only consuming around 1 W of power per wheel. This size of reaction wheel is common amongst 6U CubeSats and can generate sufficient torque to meet the mission’s attitude control parameters as indicated by Appleton’s disturbance torque equations.

Furthermore, these reaction wheels are power and weight efficient, which is especially important since wheels must be constantly active, and we are using three wheels in our design.



Figure 10: RWP050 Reaction Wheel

Parameter	Value
Angular Momentum Storage	0.05 N m s
Maximum Torque	0.007 N m
Mass	0.24 kg
Max Power	< 1.0 W

Voltage	10 to 14 V
Dimensions	58 X 25 X 58 mm

Table 4: RWP050 Specifications

3.3.2. Sensor Selection

While the actuators selected may be able to impart the torque required to detumble and maintain proper spacecraft attitude, active satellite control cannot be sustained without accurate and up to date knowledge of Appleton's movement and orientation. The following components make up the suite of on-board sensors which Appleton will use in conjunction with filtering and estimation algorithms to determine its attitude and angular velocity in space.

Unlike the actuators considered for this subsystem, most sensors we reviewed while compiling our attitude determination suite came at comparatively low cost to Appleton's mass and power budgets. This is to say that when selecting attitude determination sensors, the mass and power requirements of the prospective components were neglected to give weight to more mission critical variables. The variables pertinent to Appleton's mission success were the accuracy and the dependability of the technology. The following sensors were selected with this reasoning in mind.

3.3.3. Gyroscope

The gyroscope we landed on was once again a component that had been chosen by the 2020 mission. The Analog Devices ADXRS453 Gyroscope has significant flight heritage and high accuracy, all while being contained in a compact, lightweight, and low power chip. When

selecting a gyroscope, the most crucial variable was the accuracy of the device, and the ADXRS453 proved to be state-of-the-art in market comparisons.

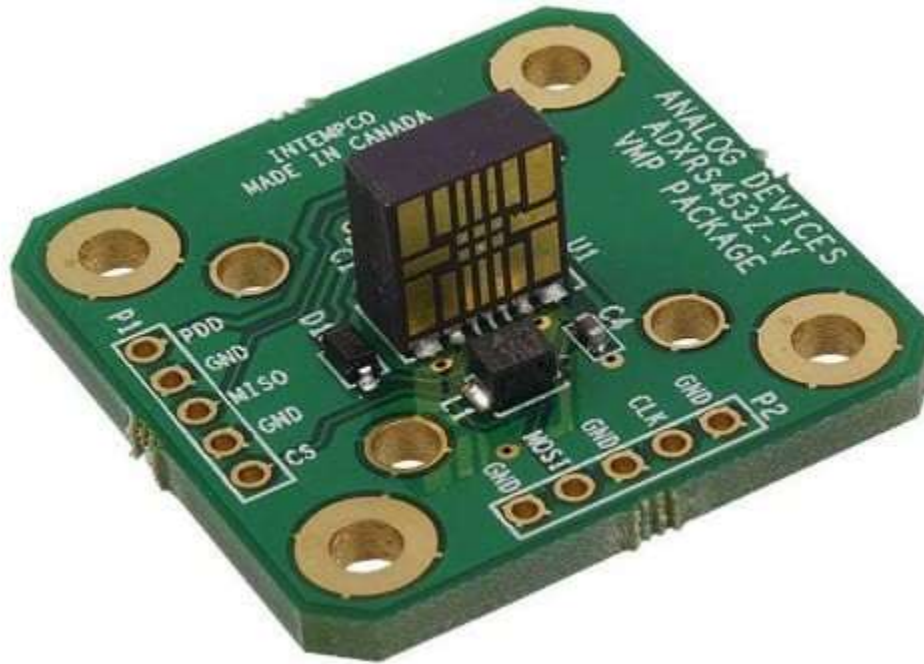


Figure 11: ADXRS453 Gyroscope

Parameter	Value
Rate Noise Density	0.015 deg/sec/ $\sqrt{\text{Hz}}$
Voltage	<5.25 V
Operating Temperature	-40 C to 105 C
Bandwidth	77.5 Hz

Table 5: ADXRS453 Specifications

3.3.4. Magnetometer

Our magnetometer came in adjunct to the magnetorquer board but proved to be a competitive piece of technology when compared to other magnetometers in the market. The

magnetometer in question is the XEN1210 Magnetometer produced by Sensixs and is extremely durable and high precision.



Figure 12: XEN1210 Magnetometer

Parameter	Value
Heading Noise	0.125 deg/ $\sqrt{\text{Hz}}$
Voltage	3.3 V
Operating Temperature	-40 C to 125 C
Dimensions	1.4 X 1.6 X 4 mm

Table 6: XEN1210 Specifications

3.3.5. Sun Sensors

Proper spacecraft attitude determination requires stable reference points similar to mankind's original orientation methods used on Earth. For this reason, a crucial part of an Earth-orbiting spacecraft's attitude knowledge comes from its orientation in relation to the Sun. Sun sensors are used in the attitude determination of most satellites and can be broken down into two distinct subgroups. Fine Sun Sensors are high precision devices used for sun vectoring with low margins of error, making them the primary supplier of knowledge informing spacecraft maintenance and pointing maneuvers. Coarse Sun Sensors on the other hand are less technically

complex and have higher vectoring error, making them ideal as for mission requirements which require less accuracy such as sun acquisition or solar array pointing.

Since Appleton will be operating in a sun-synchronous orbit, we know that one face of the spacecraft will have ideal sun vectoring capabilities for most of the mission, while the opposite face will have minimal contact with the sun over the course of the mission. Because of this orbital placement, it was determined to use a 5-sensor suite for Appleton's sun vectoring design. The Fine Sun Sensor we have selected happens to be the same model that was used in last year's project as it remains a state-of-the-art sensor. The Coarse Sun Sensor was also considered last year and is ideal for our suite design based on its low weight and power consumption.



Figure 13: NFSS-411 Fine Sun Sensor

Parameter	Value
Mass	<35 g
Power Consumption	37.5-130 mW
Accuracy	<0.1 degree
Sampling Rate	5 Hz
Field of View	140 degrees

Table 7: NFSS-411 Specifications



Figure 14: Hyperion SS200 Coarse Sun Sensor

Parameter	Value
Mass	3 g
Power Consumption	2.5-40 mW
Accuracy	<1 degree (+/- 45 degree range)
Sampling Rate	<100 Hz

Field of View	110 degrees
---------------	-------------

Table 8: SS200 Specifications

3.3.6. Accelerometer

The accelerometer we decided on is the STM IIS3DHHHC produced by ST Microelectronics. This 3-axis linear accelerometer offers competitive analogue accuracy with high durability and especially low noise in readings.

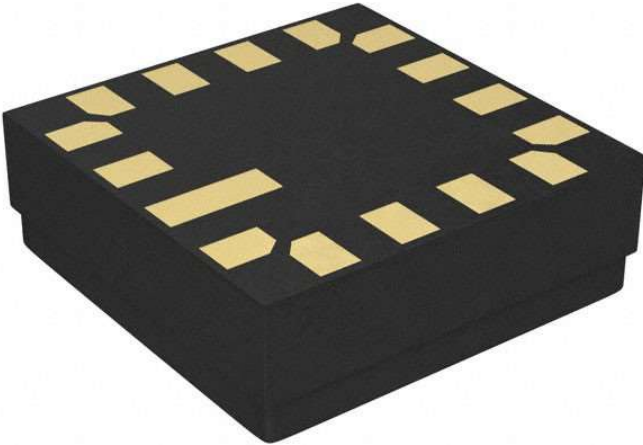


Figure 15: STM IIS3DHHHC Accelerometer

Parameter	Value
Full Scale	+/-2.5 g
Float	16-bit
Operating Temperature	-40 C to 85 C

Noise	45 $\mu\text{g}/\sqrt{\text{Hz}}$
-------	-----------------------------------

Table 9: IIS3DHHC Specifications

3.3.7. GPS

The GPS we decided on is the built-in GPS that accompanies our on-board computer (the Kyten-M3 Plus). This GPS was chosen because of its simplicity and guarantee of its compatibility with our on-board computer.

Parameter	Value
Position Accuracy	<10 m RMS
Velocity Accuracy	<1 m/s RMS

Table 10: Kyten-M3 Plus GPS Specifications

3.4. Detumbling

As discussed in the mission requirements section of this chapter, Appleton must successfully detumble after release from the launch vehicle before proceeding with the rest of its mission. In the actuator selection section, we briefly described how magnetorquers can be used to impart torque on the spacecraft body by interacting with the geomagnetic field. In this section we will break down the physics behind this process and explain how this actuation system can be integrated into a closed loop control system to successfully detumble our satellite.

Appleton's detumbling can be defined by the relationship between the magnetic dipole generated by the spacecrafts magnetorquers and the body-fixed geomagnetic field. The control torque imparted on the satellite due to the relationship between these two field vectors can be summed up in the equation below:

$$\vec{L} = \vec{m} \times \vec{B} \quad (2)$$

Where m is the magnetic dipole vector and B is the field vector. Since the control torque is equal to the cross product of these two vectors, we know that vector \vec{L} must be orthogonal to the plane on which vectors \vec{m} and \vec{B} lie. This is better described in the diagram of a satellite rotating about axis 'm' seen in Figure 16:

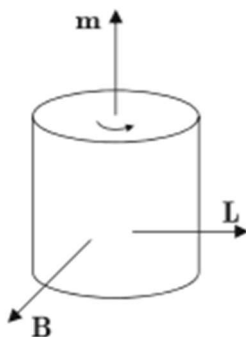


Figure 16: FBD of Appleton's Geomagnetic Attitude Control

This highlights an important consideration in the design of an ADCS system that relies on magnetorquers to detumble. Due to the configuration of the Earth's magnetic field, the spacecraft's orbit can have a significant effect on the ability of magnetorquers to function in all three axes. Since it is necessary for the geomagnetic field vector to be orthogonal to the magnetic dipole generated by the magnetorquers, certain orbits – namely orbits that lie in the geomagnetic equatorial plane – would not enable control torque about all three axes. Fortunately, the nearly polar sun-synchronous orbit Appleton will be placed in should allow for full magnetorquer control, with the highest torque present in the y-axis as seen in the drawing below:

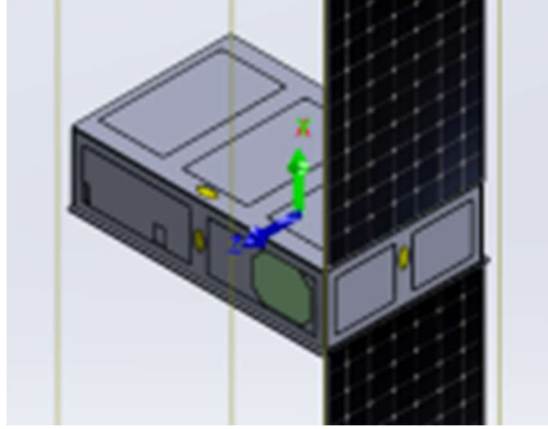


Figure 17: Attitude Configuration of Appleton

Considering the torque equation discussed above, we can begin to develop a control law around this relationship to successfully detumble our satellite. The theory commonly used in magnetorquer actuated detumble controllers is known as the ‘B-dot algorithm,’ where ‘B-dot’ refers to the rate of change in the magnetic field over time. To understand how this algorithm gets its name and its effectiveness in detumbling satellites, we first must break down the equation that defines the magnetic dipole moment generated by a magnetorquer.

$$\vec{m} = \frac{k}{\|\vec{B}\|} (\vec{\omega} \times \vec{b}) \quad (3)$$

Where

$$k = \frac{4\pi}{P} (1 + \sin(\alpha)) J_{min} \quad (4)$$

$$\vec{b} = \frac{\vec{B}}{\|\vec{B}\|} = \frac{\vec{B}}{\sqrt{\sum_{k=1}^3 |B|^2}} \quad (5)$$

As seen in the above formula, the magnetic dipole moment of a magnetorquer can be expressed in terms of the angular velocity of the satellite, along with the local geomagnetic field

strength and the satellites orbital information expressed in the gain function. If no angular velocity data is available (which would be unlikely for most satellite missions) an equivalent expression can be derived using B-dot as seen below, where k is the same as defined above.

$$\vec{m} = \frac{k}{\|\vec{B}\|} (\dot{\vec{B}}) \quad (6)$$

However, it is important to note that this function cannot be proven to be globally asymptotically stable as with the previous equation but can be used to successfully detumble a satellite to a comparable degree of accuracy.

Understanding the variables that go into the magnetic dipole allows us to better analyze the stability of a detumble control system constructed around the control torque equation discussed earlier. As seen in the equation below, we can combine the control torque equation with the formula describing the magnetic dipole for a more comprehensive view of detumble control. This expression can then be restated using an identity matrix as seen in the equation below:

$$\vec{L} = \vec{m} \times \vec{B} = -k(I_3 - \vec{b}\vec{b}^T)\vec{\omega} \quad (7)$$

This simplified form allows us to better prove the stability of this control theory using a Lyapunov function. The equation we choose as our Lyapunov candidate function needs to reflect the motion being controlled in the detumble process. Therefore, the candidate function we use is the equation for the rotational kinetic energy of the satellite.

$$V = \frac{1}{2} \vec{\omega}^T J \vec{\omega} \quad (8)$$

Taking the derivative of the candidate function resembles our simplification of the torque equation as seen below:

$$\dot{V} = -k\vec{\omega}^T(I_3 - \vec{b}\vec{b}^T)\vec{\omega} \quad (9)$$

Since the eigenvalues of the matrix $(I_3 - \vec{b}\vec{b}^T)$ would always be 0, 1, and 1, it can be assumed that this part of equation to be positive semi-definite. Considering the rest of the V-dot function, it is clear that the Lyapunov derivative is negative semi-definite, as is required for system stability. The rate of change in rotational kinetic energy becomes zero as omega approaches zero, as well as when the omega vector and geomagnetic field vector are parallel. This accurately describes a magnetorquer control system as the satellite will not be able to provide detumble torque when the magnetic field is not orthogonal to the axis of rotation, as discussed previously. Once the stability of our model has been proven we can design a detumble control system around it. A simple feedback control design commonly used with the 'B-dot' algorithm is known as a 'Bang-bang' controller. The equation below represents the second half of our bang-bang control model, with the first half originating in our definition of the magnetic dipole m in the equation above.

$$m = \sum_{t=1}^3 -m_i^{max} \sin(\vec{u}_i \cdot \vec{B}) \quad (10)$$

As you can infer from the above expression, our bang-bang controller relies on binary inputs in voltage, where m_i^{max} represents the magnetic dipole generated when the magnetorquer is operating at full capacity. This reduces system complexity and requires minimal additional coding be done on the magnetorquer board. Aside from being computationally efficient, bang-

bang control systems are ideal for the discrete time modelling used in our project and can be tuned to have comparable accuracy to more computationally complex PD or PID controllers.

3.5. Attitude Determination

As discussed in the mission requirements section of this chapter, Appleton must obtain consistent and accurate attitude knowledge over the duration of the mission for operational success. On typical satellite missions, this goal is accomplished via a suit of onboard sensors through processes known as deterministic algorithms. Another set of methods used to determine satellite attitude are known as recursive algorithms. These use discrete time to estimate the satellites' orientation based on previous attitude data.

For the purposes of this project, we will be using both deterministic and recursive algorithms to provide us with accurate data on Appleton's theoretical attitude. We will cover the use of recursive algorithms to filter attitude data in a later section, but first we must understand the deterministic algorithms that are used to obtain orientation data from our onboard sensors.

3.5.1. TRIAD

The TRIAD or Tri-axial Attitude Determination algorithm was developed in 1964 by Harold Black and was intended to be used by the U.S. Navy for satellite and ground-based navigation. TRIAD was one of the first solutions to the problem of spacecraft attitude determination and remains the basis for most deterministic attitude algorithms used on-board satellites today. The TRIAD algorithm is also well known for its simplicity and computational efficiency, which may help explain the wide usage of this algorithm and its derivations in the attitude control systems of most modern satellites.

The TRIAD method uses solar and magnetospheric vectoring to estimate satellite orientation. To accomplish this, four pieces of information are required: a body-fixed sun vector, a body-fixed magnetospheric vector, a Earth-fixed or inertial sun vector, and an inertial magnetospheric vector. The two inertial vectors represent the reference frame, and the two body fixed vectors describe the on-board readings from the satellites sun sensors and magnetometer, respectively. For the purpose of this project, the reference sun vector will be obtained using an equation which calculates the position of the Earth based on the Julian calendar date as reflected in this expression.

$$\begin{aligned}
 JD(Y, M, D, h, m, s) &= 1721013.5 + 367Y \\
 &- INT \left\{ \frac{7}{4} \left[Y + INT \left(\frac{(M + 9)}{12} \right) \right] \right\} + INT \left(\frac{275M}{9} \right) + D \\
 &+ \frac{(60h + m + \frac{s}{60})}{1440}
 \end{aligned} \tag{11}$$

The reference magnetospheric data is found by referencing the World Magnetic Model (WMM) which is updated every year by the NOAA and requires only the longitude, latitude, and altitude of a satellite to determine its inertial magnetospheric vector.

The overarching goal of TRIAD is to allow for a spacecraft's body-fixed frame to be rotated into the Earth-fixed inertial frame to obtain an estimate of the satellite's orientation in quaternions. To accomplish this, TRIAD sets out to find an attitude matrix, which is a DCM that can accurately describe the satellite's body frame in terms of the inertial reference frame (ECI). Since we are using both sun and magnetospheric vectors to adjust frames, we need to acknowledge this in our calculation of the attitude matrix. Ideally this matrix would be the same for rotating the frames from both vector sources, but since the sensors have varying levels of

accuracy, TRIAD must weigh their vector inputs based on relative precision. To reiterate, the equation below is true only under ideal conditions when sensor noise is not present, but accurately reflects the central concept behind the TRIAD algorithm.

$$Ar_i = b_i \quad (12)$$

Here the ‘ i ’ is equal to either 1 or 2. In the following equations a subscript of 1 connotes the sensor with the more accurate readings while 2 represents the sensor with the less accurate readings. In the context of our project, the sun vectoring suite would provide us with slightly more accurate data than our magnetometer.

Once we have established the sources of our measurement and reference vectors, we can form two orthonormal ‘triads’ of vectors. As seen below, one triad depicts the reference frame, and the other triad depicts the measurement or observation frame.

$$M_{obs} = \left[b_1, \frac{b_1 \times b_2}{|b_1 \times b_2|}, b_1 \times \frac{b_1 \times b_2}{|b_1 \times b_2|} \right] \quad (13)$$

$$M_{ref} = \left[r_1, \frac{r_1 \times r_2}{|r_1 \times r_2|}, r_1 \times \frac{r_1 \times r_2}{|r_1 \times r_2|} \right] \quad (14)$$

From here, we can find a DCM that correctly rotates the Earth reference frame into the spacecraft's body-fixed frame by substituting M_{ref} and M_{obs} for r and b in equation 12 and solving for A .

$$AM_{ref} = M_{obs} \quad (15)$$

$$A = M_{obs}M_{ref}^T \quad (16)$$

Finally, expanding out our triads and simplifying gives us an equation for the attitude matrix which can be used to find a static estimate of the satellite's orientation in quaternions.

$$\begin{aligned}
A_{DCM} = b_1 r_1^T \left(b_1 \times \frac{b_1 \times b_2}{|b_1 \times b_2|} \right) \left(r_1 \times \frac{r_1 \times r_2}{|r_1 \times r_2|} \right)^T \\
+ \left(\frac{b_1 \times b_2}{|b_1 \times b_2|} \right) \left(\frac{r_1 \times r_2}{|r_1 \times r_2|} \right)^T
\end{aligned} \tag{17}$$

One of the key problems with TRIAD is that it requires the satellites' body fixed vectors to be normalized, which neglects the noise present in the sensor input, causing substantial inaccuracy. The problem of sensor input error was addressed by Grace Wahba and the subsequent solutions to her problem have become widely used attitude determination algorithms.

3.5.2. Wahba's Question

In 1965 Grace Wahba sought [22] a method to find a rotational matrix between two coordinate systems, those coordinate systems being the fixed frame and reference frame of the observed body, this is now known as Wahba's Problem. When given the two unit vectors $\{r_1, r_2, \dots, r_n\}$ and $\{b_1, b_2, \dots, b_n\}$ with $n \geq 2$, it is necessary to find the rotational matrix A which minimizes the loss function:

$$L(A) = \frac{1}{2} \sum_{i=1}^n \|b_i - Ar_i\|^2 \tag{18}$$

In this r represents the reference matrix and b represents the observation matrix.

Expanding the equation $\|b_i - Ar_i\|^2$ results in:

$$\|b_i - Ar_i\|^2 = \|b_i\|^2 + \|Ar_i\|^2 - 2b_i \cdot (Ar_i) = 2 - 2tr(Ar_i b_i^T) \tag{19}$$

Within this equation the b_i^T is the transpose of the b_i matrix and tr represents the trace of $Ar_i b_i^T$ as the last term in this equation is the only one dependent on the A matrix it is possible to minimize equation 18 by finding the A matrix that maximizes:

$$F(A) = \text{tr}(Ar_i b_i^T) \quad (20)$$

Since the mission has two reference and two observation vectors it is possible to rewrite equation 18 such that:

$$L(A) = \frac{1}{2} \sum_{i=1}^2 a_i \|b_i - Ar_i\|^2 \quad (21)$$

Here a_i represents the weight applied to each sensor with a_1 corresponding to b_1 and a_2 corresponding to b_2 . Using (EQ#) and (EQ#) it is possible to rewrite the loss function as:

$$L(A) = \frac{1}{2} \sum_{i=1}^2 a_i - \text{tr}(AB^T) \quad (22)$$

Where in B is defined as:

$$B = \sum_{i=1}^2 a_i b_i r_i^T \quad (23)$$

To solve this problem, we used both Davenport's q-Method as well as the QUEST method which is discussed in more detail in the coming sections.

3.5.3. Davenport's q-Method

One of the first major solutions to Wahba's Problem was proposed by Paul Davenport in 1968, now known as Davenport's q-Method. Davenport's q-Method states that if you have quaternions in the form:

$$\mathbf{q} = \begin{bmatrix} q_1 \\ q_2 \\ q_3 \\ q_4 \end{bmatrix} \quad (24)$$

Where:

$$\|\mathbf{q}\| = 1 \quad (25)$$

Then it is possible to represent the A matrix in the form of a homogenous quadratic function bound by q :

$$A = (q_4^2 - |\mathbf{q}_{1:3}|^2)I + 2\mathbf{q}_{1:3}\mathbf{q}_{1:3}^T - 2q_4[\mathbf{q}_{1:3}^\times] \quad (26)$$

This can then be rewritten as:

$$\text{tr}(AB^T) = \mathbf{q}^T K \mathbf{q} \quad (27)$$

Where K is defined as:

$$K = \begin{bmatrix} S - I_3 \text{tr}B & \mathbf{z} \\ \mathbf{z}^T & \text{tr}B \end{bmatrix} \quad (28)$$

Where:

$$S = B + B^T \quad (29)$$

$$z = \begin{bmatrix} B_{23} - B_{32} \\ B_{31} - B_{13} \\ B_{12} - B_{21} \end{bmatrix} = \sum_{i=1}^2 a_i b_i \times r_i \quad (30)$$

It can then be shown that:

$$K \hat{q} = \lambda_{max} \hat{q} \quad (31)$$

In this equation λ represents the eigenvalues of K resulting from the greatest eigenvalues. One of the major disadvantages produced by this method is the computational load required to find the optimal eigenvalues and eigenvectors. To overcome this disadvantage, we then used the QUEST method.

3.5.4. QUEST

The Quaternion Estimator (QUEST) algorithm was developed in 1979 in collaboration with the NASA's MagSat mission. The high refresh rate required by the MagSat mission demanded an algorithm that was less computationally dense than Davenport's q-Method, which had been used by NASA on several preceding satellites. The QUEST algorithm's efficiency can be attributed to the way in which it replaced the iterative 4 X 4 matrix operations used in Davenport's q-Method with iterative scalar computations combined with simple matrix multiplications. Though QUEST is theoretically less robust than the q-Method, it has proven to be extremely robust in practical applications. Since the launch of MagSat, the QUEST algorithm has quickly become the most widely used spacecraft attitude control algorithm used to as a solution to Wahba's problem.

To find the maximum eigenvector λ_{max} more efficiently, the QUEST algorithm first restates equation 27 from Davenport's q-Method into two separate equations.

$$[(\lambda_{max} + trB)I_3 - S]\hat{q}_{1:3} = \hat{q}_4 z \quad (32)$$

$$(\lambda_{max} + trB)\hat{q}_4 - \hat{q}_{1:3} = 0 \quad (33)$$

These equations can then be recombined to solve for q using adjoint matrix form since we know the adjoint of a matrix divided by the matrix's determinant is equal to the inverse of the matrix as seen in the equation below.

$$\begin{aligned} q_{1:3} &= q_4 [(\lambda_{max} + trB)I_3 - S]^{-1} z \\ &= \frac{(q_4 \text{adj}((\lambda_{max} - trB)I_3 - S)z)}{\det((\lambda_{max} - trB)I_3 - S)} \end{aligned} \quad (34)$$

To further simplify these matrix alterations, we can use the Cayley-Hamilton theorem. This states that all real square or complex matrices satisfy their characteristic polynomials. Since this definition applies to classical adjoint matrices as well as the quaternionic matrices that are central to the QUEST algorithm, we know that the Cayley-Hamilton theorem applies to equation 34 and allows us to find the equation for the optimal quaternion estimate as seen below.

$$q = \alpha \left[\frac{\text{adj}(\rho I_3 - S)z}{\det(\rho I_3 - S)} \right] \rho = \lambda_{max} + trB \quad (35)$$

This equation provides us with the static quaternion estimate that we need from QUEST assuming we know the λ_{max} , which is the solution to the characteristic equation of the K -matrix seen in equation 31. For systems with more than one observation vectors as in the case will Appleton's design, solving for the maximum eigenvalue of the characteristic equation can become more complicated. Fortunately, the characteristic equation for the K -matrix has a simple closed-form solution to answer Wahba's Problem when specifically, two observation vectors are present as in the case of Appleton's ADCS. Having two observations allows for several

simplifications which finally give us with expression for λ_{max} complete with TRIAD weighting variables as seen below.

$$\lambda_{max} = a_1^2 + a_2^2 + 2a_1a_2[(b_1 \cdot b_2)(r_1 \cdot r_2) + \|b_1 \times b_2\| \|r_1 \times r_2\|]^{\frac{1}{2}} \quad (36)$$

While maintaining some of the definitions found in Davenport's q-Method, the QUEST algorithm will be the main workhorse in Appleton's attitude determination code. This code will be written in MATLAB's language and integrated directly into a function block in the Simulink file which will be discussed in a later section.

It should be noted that the Rodriguez parameter present in QUEST makes it unable to represent 180-degree rotations. Past projects have tried using the Estimator of the Optimal Quaternion (ESOQ) algorithm to correct for this, but for the purpose of our mission requirements we have chosen to forego this.

3.6. ATTITUDE CONTROL

3.6.1. Reaction Wheel Sizing

Appleton's reaction wheels must be capable of counteracting all disturbance torques imparted by the environment in orbit. As discussed in the Component Selection chapter of this report, the most critical disturbance torque that must be considered for Appleton's ADCS design is the aerodynamic torque due to periods of low altitude orbit. This torque can be expressed by the equation below.

$$T_a = \frac{1}{2} \rho C_d A_s V^2 (C_{pa} - C_g) \quad (37)$$

Where C_{pa} is the center of aerodynamic pressure, C_g is the center of gravity, V is Appleton's velocity, ρ is the atmospheric density, and C_d is the drag coefficient. Another important disturbance torque that needs to be considered is the torque due to gravity, which is expressed in the following expression.

$$T_g = \frac{3M}{2R^2} |I_x - I_y| \sin(2\theta) \quad (38)$$

Where M and R are the mass and radius of the Earth respectively, and θ is equal to approximately 5 degrees or 0.0872 radians. The next disturbance torque is much less significant and is much more critical for smaller satellites. This is the torque due to solar pressure is defined in the equation below.

$$T_{sp} = F(C_{ps} - C_g) \quad (39)$$

Where:

$$F = \frac{F_s}{c} A_s (1 + q) \cos(l) \quad (40)$$

And where F_s is the solar flux constant, c is the speed of light, q is the coefficient of reflection, C_{ps} is the center of solar pressure, and A_s is the surface of the RAM facing surface. The final disturbance torque also has minimal effect on Appleton's attitude control. This is the torque due to the satellites electrical systems interacting with the Earth's geomagnetic field and is expressed in the equation below. Here B represents the Earth's magnetic field and D represents Appleton's residual dipole.

$$T_m = DB \quad (41)$$

Considering all the above disturbance torques we can then ensure that our reaction wheels are capable of meeting Appleton's mission requirements in terms of their actuating torque by comparing the maximum disturbance torque along any one axes to the control torque equations below.

$$\dot{h} = -\hat{\omega} \times h - \hat{L} \quad (42)$$

$$L = -k_p(\hat{q}_4)\delta\hat{q}_{1:3} - k_d(1 \pm \hat{q}_{1:3}^T\hat{q}_{1:3})\hat{\omega} \quad (43)$$

Substituting the angular momentum our chosen reaction wheels are capable of imparting along with angular velocity characteristics allows us to ensure that the satellite will have sufficient torque authority over any of the disturbance torques described in this section.

3.6.2. Extended Kalman Filter

In order to use the Extended Kalman Filter we first had to find the state vector. The rotation of the satellite is given by:

$$\boldsymbol{\omega} = \begin{bmatrix} \omega_x \\ \omega_y \\ \omega_z \end{bmatrix} \quad (44)$$

The quaternions representing the three Euler angles and a fourth term used to avoid singularities are given by:

$$\boldsymbol{q} = \begin{bmatrix} q_1 \\ q_2 \\ q_3 \\ q_4 \end{bmatrix} \quad (45)$$

Using equations 44 and 45 we can find the true state vector to be:

$$\mathbf{X}_{true} = \begin{bmatrix} \omega_x \\ \omega_y \\ \omega_z \\ q_1 \\ q_2 \\ q_3 \\ q_4 \end{bmatrix} \quad (46)$$

It is then necessary to find the angular velocity as defined by:

$$\alpha = \dot{\omega}_x \mathbf{i} + \dot{\omega}_y \mathbf{j} + \dot{\omega}_z \mathbf{k} + (\boldsymbol{\Omega} \times \boldsymbol{\omega}) \quad (47)$$

Within this equation $\boldsymbol{\Omega}$ is the angular velocity in terms of the reference frame. When the reference frame and body frame are the same the last term disappears, this allows the angular acceleration to be found with just the angular velocity components. As the time derivative of each angular velocity is unknown, it is possible to find the angular accelerations with the net torque and the Euler's Equation:

$$\boldsymbol{\tau}_{net} = \dot{\mathbf{H}}_{rel} + (\boldsymbol{\omega} \times \mathbf{H}) \quad (48)$$

In this equation \mathbf{H} represents the angular velocity and J represents the moment of inertia of the spacecraft with the subscript specifying the x, y, z coordinates.

$$\mathbf{H} = J_x \omega_x \mathbf{i} + J_y \omega_y \mathbf{j} + J_z \omega_z \mathbf{k} = J\boldsymbol{\omega} \quad (49)$$

$$\dot{\mathbf{H}}_{rel} = J_x \dot{\omega}_x \mathbf{i} + J_y \dot{\omega}_y \mathbf{j} + J_z \dot{\omega}_z \mathbf{k} = J\boldsymbol{\alpha} \quad (50)$$

Then substituting equations 49 and 50 into 48 we get

$$(\boldsymbol{\mu} \times \mathbf{B}) = J\boldsymbol{\alpha} + (\boldsymbol{\omega} \times J\boldsymbol{\omega}) \quad (51)$$

Solving for the angular velocity we find:

$$\alpha = J^{-1}[(\mu \times B) - (\omega \times J\omega)] \quad (52)$$

The next portion of the dynamical system is the kinematics of the quaternions:

$$\frac{d}{dt}(\mathbf{q}) = \frac{1}{2}\Omega(\omega)\mathbf{q} \quad (53)$$

Where $\Omega(\omega)$ is the cross matrix of the angular velocity about the body frame and is defined by:

$$\Omega(\omega) = \begin{bmatrix} 0 & \omega_z & -\omega_y & \omega_x \\ -\omega_z & 0 & \omega_x & \omega_y \\ \omega_y & -\omega_x & 0 & \omega_z \\ -\omega_x & -\omega_y & -\omega_z & 0 \end{bmatrix} \quad (54)$$

Substituting equations 53 and 54 into equation 46 it is possible to find the derivative of the state space vector as:

$$\frac{d}{dt}\mathbf{X} = \begin{bmatrix} \dot{\omega}_x \\ \dot{\omega}_y \\ \dot{\omega}_z \\ \dot{q}_1 \\ \dot{q}_2 \\ \dot{q}_3 \\ \dot{q}_4 \end{bmatrix} = \begin{bmatrix} J^{-1}[(\mu \times B) - (\omega \times J\omega)] \\ \frac{1}{2}\Omega(\omega)\mathbf{q} \end{bmatrix} \quad (55)$$

It is then necessary to use Taylor Series approximation to linearize the derivative of the state space vector. The expanded vector form of the state space vector is:

$$\dot{\mathbf{X}} = f(\mathbf{X}, \mathbf{u}) = \begin{bmatrix} -\frac{1}{I_{xx}}(B_y\mu_z - B_z\mu_y - I_{yy}\omega_y\omega_z + I_{zz}\omega_y\omega_z) \\ \frac{1}{I_{yy}}(B_x\mu_z - B_z\mu_x - I_{xx}\omega_x\omega_z + I_{zz}\omega_x\omega_z) \\ -\frac{1}{I_{zz}}(B_x\mu_y - B_y\mu_x - I_{xx}\omega_x\omega_y + I_{yy}\omega_x\omega_y) \\ \frac{1}{2}(q_4\omega_x - q_3\omega_y + q_2\omega_z) \\ \frac{1}{2}(q_3\omega_x + q_4\omega_y - q_1\omega_z) \\ \frac{1}{2}(-q_2\omega_x + q_1\omega_y + q_4\omega_z) \\ \frac{1}{2}(-q_1\omega_x - q_2\omega_y - q_3\omega_z) \end{bmatrix} \quad (56)$$

Where u is the control input and μ is the magnetic moment vector. The Taylor Series for the state space can be written as:

$$f(x) = f(x_0, u_0) + \Delta_x f(x_0, u_0)(x - x_0) \quad (57)$$

Within this system the Jacobian Matrix can then be written as:

$$\Delta_x f(\mathbf{X}, \mathbf{u}) = \begin{bmatrix} -J^{-1}[\omega^\times]J & 0_{3 \times 4} \\ \frac{1}{2}\Xi(q) & \frac{1}{2}\Omega(\omega) \end{bmatrix}$$

$$= \begin{bmatrix} 0 & \frac{\omega_z(I_{yy} - I_{zz})}{I_{xx}} & \frac{\omega_y(I_{yy} - I_{zz})}{I_{xx}} & 0 & 0 & 0 & 0 \\ -\frac{\omega_z(I_{xx} - I_{zz})}{I_{yy}} & 0 & -\frac{\omega_x(I_{xx} - I_{zz})}{I_{yy}} & 0 & 0 & 0 & 0 \\ \frac{\omega_y(I_{xx} - I_{yy})}{I_{zz}} & \frac{\omega_x(I_{xx} - I_{yy})}{I_{zz}} & 0 & 0 & 0 & 0 & 0 \\ \frac{q_4}{2} & -\frac{q_3}{2} & \frac{q_2}{2} & 0 & \frac{\omega_z}{2} & -\frac{\omega_y}{2} & \frac{\omega_x}{2} \\ \frac{q_3}{2} & \frac{q_4}{2} & -\frac{q_1}{2} & -\frac{\omega_z}{2} & 0 & \frac{\omega_x}{2} & \frac{\omega_y}{2} \\ -\frac{q_2}{2} & \frac{q_1}{2} & \frac{q_4}{2} & \frac{\omega_y}{2} & -\frac{\omega_x}{2} & 0 & \frac{\omega_z}{2} \\ -\frac{q_1}{2} & -\frac{q_2}{2} & -\frac{q_3}{2} & -\frac{\omega_x}{2} & -\frac{\omega_y}{2} & -\frac{\omega_z}{2} & 0 \end{bmatrix} \quad (58)$$

$$= \mathbf{A}$$

To start the actual Extended Kalman Filter it is necessary to set the nonlinear plant equation as:

$$\mathbf{X}^{true} = f(\mathbf{X}^{true}, \mathbf{u}, \omega, t) \quad (59)$$

Where \mathbf{X} is the ideal value of the state vector, u is the control input, w is the process noise, and t is the system time. Using the above plant, it is possible to model the state measurement as:

$$y = h(\mathbf{X}^{true}) + v \quad (60)$$

In which v is the sensor noise, h is a nonlinear function relating the state vector to the sensor measurement. Quaternions one through three are found through the spacecraft gyroscope

and a virtual fourth quaternion is found via the TRIAD method, equation 60 can then be rewritten as:

$$y = C\mathbf{X}^{true} + v \quad (61)$$

In this equation C represents a seven dimensional matrix.

It is then necessary to find the estimation error covariance as defined by:

$$\dot{P} = AP + PA^T + Q \quad (62)$$

Where Q is the process error covariance matrix and R is the measurement error covariance matrix. We then found that the initial P values were:

$$P_0 = Qdt \quad (63)$$

It is then possible to find the Kalman gain as:

$$K = PC^T R^{-1} \quad (64)$$

We then updated the state estimate as:

$$\dot{\hat{\mathbf{X}}} = f(\hat{\mathbf{X}}, \hat{\mathbf{u}}) + K(y - C\hat{\mathbf{X}}) \quad (65)$$

As a continuous-discreet Kalman filter it is possible to define the initial state estimation as:

$$\hat{\mathbf{X}} = f(\hat{\mathbf{X}}, \hat{\mathbf{u}}, \boldsymbol{\omega}, t) \quad (66)$$

And the Initial error covariance as:

$$\dot{P} = AP + PA^T + Q \quad (67)$$

Then calculating the Kalman gain as:

$$\hat{X}^+ = \hat{X}^- + K[y - C\hat{X}^-] \quad (68)$$

Where in the (+) represents the update value and (-) represents the initial values of each time step. The error covariance is then updated as:

$$P^+ = [I - KC]P^- \quad (69)$$

3.6.3. STK

Though the active simulation and testing of Appleton's attitude determination and control subsystem are still in progress at the time of writing, the theory behind the simulation design is described here. System's Tool Kit (STK) is a physics-based modeling software used throughout the space industry. STK allows engineers to propagate satellite orbits, model sensors, and obtain environmental data for a variety of spacecraft missions.

In order to implement and test Appleton's ADCS design, STK was first used to propagate Appleton's orbit and obtain vectoring outputs for the deterministic attitude algorithms shown in the section on Attitude Determination. Past projects have attempted full modeling integrations between STK and the control systems designed in MATLAB/Simulink, but these attempts have usually run into significant problems with cross platform integration and have been more or less ruled unnecessary due to CubeSat specific packages added to the Simulink software.

While previous years have simply used STK for visualization and to obtain clean quaternion and omega values to be used in the STK simulation, this year we investigated obtaining vectoring data to be used directly with our QUEST algorithm. As discussed in the section on TRIAD, the observational vectors we need to calculate a static quaternion estimate are the body-fixed magnetospheric and sun vectors. With the help of the Space Environments subsystem, we were able to find a way to model and output a body-fixed magnetospheric field using STK's SEET toolbox. While we were not able to fully integrate this into our system, this strategy should be considered by future projects.

The screenshot below depicts our STK Attitude Model, complete with live quaternion and angular velocity readings, orbital information, orientation vectors, and a suite of sun sensors. These five sensors were modeled to reflect the single fine sun sensor and four coarse sun sensors that are included in our suite (Note the FOV of the sensors in the simulation below are purposefully not to scale to allow for better visualization). While sensors in STK are not designed to output vectoring data in a way that would allow us to replicate sun sensors, prior research suggests using STK's Vector Geometry Tool paired with the sensor activation periods to simulate sun-sensor outputs. While we were not able to obtain sun vectoring from STK, this would be something for future projects to consider as well.

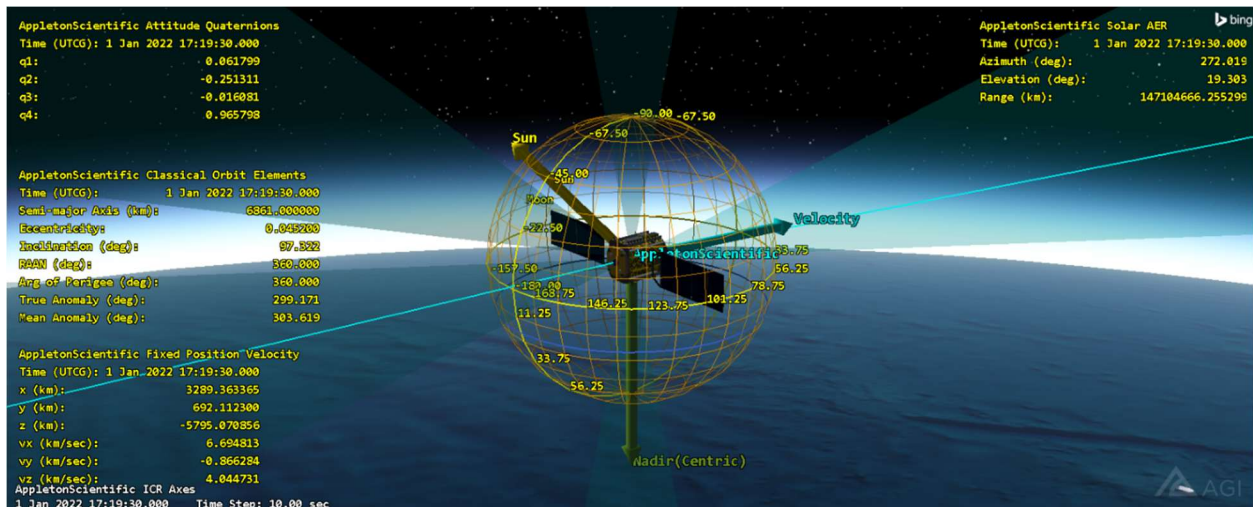


Figure 18: Appleton's STK Attitude Simulation

3.6.4. Simulink

Once again, the Simulink file is not running at the time of writing, but its design is described below. It should be noted that the control system design was broken up into two separate Simulink diagrams, which each satisfying one of Appleton's central mission objectives. The first simulation models spacecraft detumble, while the second simulates regular attitude maintenance. For the purpose of this project, Appleton's suite of onboard sensors will be simulated using STK modeling and dynamic Euler equations. This data was then run through sensor simulation blocks in a Simulink file and seeded with three axes noise to imitate real world sensor readings. This section of the simulation can be described as a 'black box' or super user information that would not be available if Appleton was in live orbit. This section can be found in both the Detumble and Maintenance control systems and incorporates the third mission requirement -- attitude determination -- into Appleton's attitude control modelling.

While both simulations include attitude determination blocks, the imported data required for each system varies slightly. Appleton's detumble system simulates only magnetometer and

gyroscope data, while it's maintenance system simulates sun-sensor, magnetometer, and gyroscope readings. Once artificial sun-sensor and magnetometer data were simulated, these were to be run through deterministic attitude determination algorithms to calculate Appleton's static quaternion estimate. Wanting to avoid the normalized noise error problems associated with the TRIAD algorithm, Appleton uses Davenport's q-Method and the QUEST algorithm by way of Wahba's Problem, as discussed in the algorithms chapter of this paper. The static quaternion estimate along with the corrupted gyroscope inputs are then run through an Extended Kalman Filter (EKF) which cleans data via discrete predictive filtering. We planned to integrate EKFs into both our detumble and maintenance control systems and compare its effectiveness against simpler low-pass filters to construct the most accurate control system based around simulated sensors.

$$J\dot{\omega} = -\omega \times J\omega + L \quad (70)$$

$$\dot{q} = \frac{1}{2}\Xi_q\omega = \frac{1}{2} \begin{bmatrix} q_4 & -q_3 & q_2 \\ q_3 & q_4 & -q_1 \\ q_2 & q_1 & q_4 \\ -q_1 & -q_2 & -q_3 \end{bmatrix} \omega \quad (71)$$

Once clean attitude and angular velocity data has been obtained, it can be sent through the detumble, and maintenance control systems whose core functions are described in the preceding chapters of this report. The outputs of these controllers are then sent to controller plant which incorporate the Equations 70 and 71 seen above. The derivative output from these plants can then feedback updated system dynamics information to the beginning of the closed loop system. While the Simulink systems do not have the inputs to properly run, their designs are reflected in Figures 19 and 20.

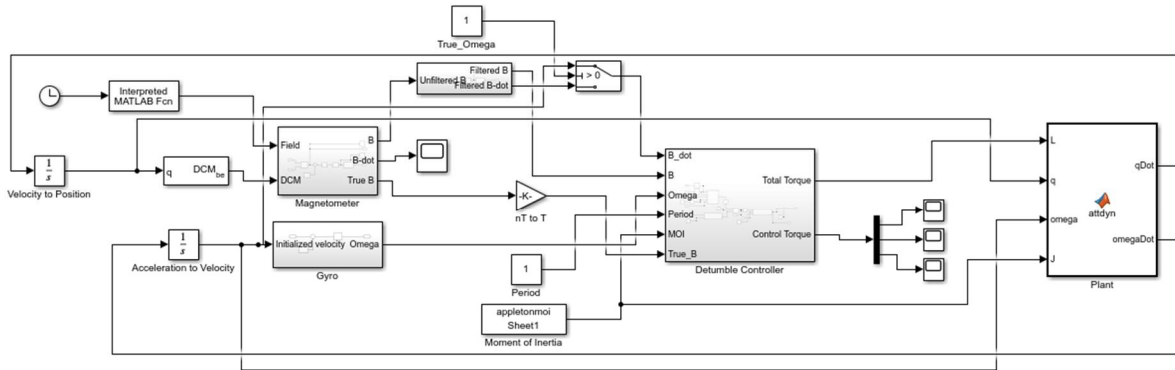


Figure 19: Detumble Simulation Diagram

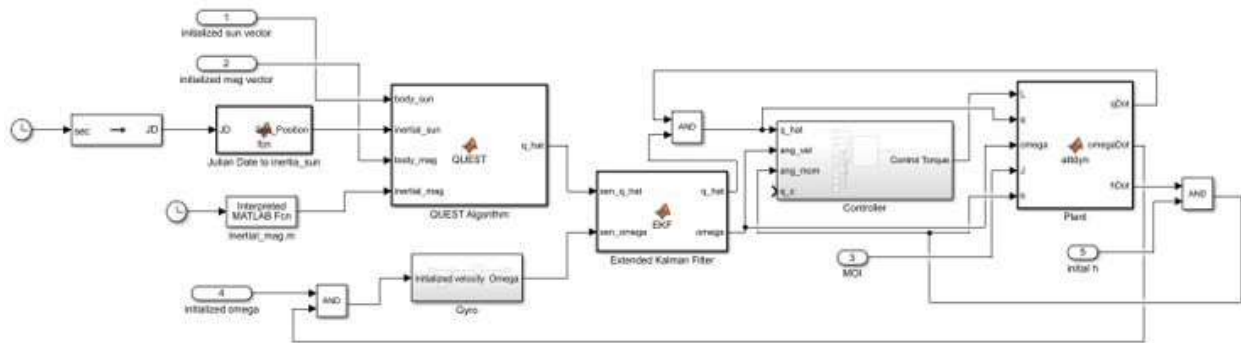


Figure 20: Maintenance Simulation Diagram

4. TELEMETRY AND COMMUNICATIONS

The telemetry and communications subsystem provides the satellite with the means to send and receive data to and from ground stations. This chapter discusses the design, analysis, and component selection process.

4.1. Overview

The telemetry and communication subsystem, also referred to as telecommunications, is responsible for transmitting and receiving data between the satellite and the ground stations. This

data is mainly scientific data collected from the two payloads onboard the satellite as well as telemetry and housekeeping information. The telecommunications system consists of a transmitter, a receiver, and an antenna. These components work together to get data to and from the satellite and ground stations. [16]

To save space onboard the satellite a transceiver was used, which combines a transmitter and a receiver into one device. Therefore, the transceiver is responsible for transmitting data from the CubeSat to ground stations (downlink) and receiving data from the ground station on the satellite (uplink). In between transmission periods data will be stored on SD cards in the onboard computer until it is ready to be transmitted. The other telecommunication component onboard the spacecraft is the antenna. The antenna is the component physically responsible for transmitting and receiving data and needs to operate at the same frequency range as the transceiver and ground stations. The antenna sends and receives data through radio waves, this frequency affects the speed of data transmission as well as the amount of power required; the higher the frequency the faster data is transmitted but the more power it uses.

Ground stations can be set up professionally by institutes such as NASA or Amazon or built by amateurs like universities or small research missions. Professional ground stations have multiple locations worldwide that allow for a larger and longer access time to the satellite, however these ground stations can come with higher costs and possible transmission limits. Amateur ground stations on the other hand don't have the restrictions of professional stations but may be impaired by a limited number of stations and therefore a lower access time and smaller transmission windows.

4.2. Component Selection

The selection of telecommunications components was started by researching previous LEO satellites requirements along with calculating data rates needed by other subsystems. The primary consideration was data requirements, radio frequency, and finally ground station compatibility. There are two main data restrictions in place for the telecommunications system, the data from the two scientific payloads (INMS and GRIDS) which have a combined data rate of 13.167 kb/s, and the instructions related to propulsion and ADCS would only be about 10 kb in size. Using these combined uplink and downlink requirements we moved on to selecting a suitable transmission frequency. These frequencies can be broken up into four main frequency ranges, as listed in the table below[]:

VHF	30 - 300 MHz
UHF	300 MHz - 3 GHz
S-Band	2 - 4 GHz
X-Band	8- 12 GHz

Table 11: Radio Frequencies

As Appleton is operating in LEO and transmitting relatively low amounts of data any of the radio frequency bands would suffice given enough access time. Therefore, to narrow our range of usable frequencies, we examined our possible ground stations. Both the AWS (Amazon Web Services) and the NASA NEN (Near Earth Network) operate mainly in S-Band and X-Band frequencies, narrowing down the selection to operate in S-Band or X-band frequencies.

[16][17][18]

4.2.1. Ground Stations

Using Systems Tool Kit (STK), a scenario was developed to model the orbit and determine access time to both the ground stations in consideration. The ground station locations were input as “Place” objects. Each of these Place objects were assigned a child Sensor object and, each sensor was assigned a Receiver object. These receivers were set to track a basic transceiver that was attached to the Satellite object. From here, the team was able to run an access time analysis for the mission duration. Comparing the two ground stations the NEN had an average time in coverage of ~16 hours a day, while the AWS resulted in an average time in coverage of ~7 hours a day.

Moving forward with NASA’s NEN the team did a more in-depth review in STK. Focusing on only NEN now the ground stations locations were mapped out and an access time analysis was run on each location, the results of which can be seen below[19]:

Location	Avg Access Time
Alaska	548.7 s
Antarctica	583.6 s
Antarctica 2	568.9 s
Australia	690.1 s
Chile	589.3 s
Florida	535.9 s
Germany	580.6 s
Hawaii	630.4 s
New Mexico	546.1 s
Norway	574.8 s
Singapore	629.9 s
South Africa	531.1 s
Sweden	557.0 s
Virginia	550.4 s

Table 12: Ground Station Access Times

The times in the table are entire scenario averages calculated by STK. For each given location, the access time could have significant variance. While the higher then average access times are better, the lower access times could cause problems if transmissions are cutoff or the transmission window is too small to receive vital housekeeping data. The small transmission windows are not a problem for downlinking of data due to the SD card on the OBC which can store up to 64GB of data onboard.

Using the average access time and minimum access time the team moved on to select a transceiver and antenna. Ultimately, the team decided on the SLink-PHY S-Band Transceiver and Patch Antenna by IQspacecom (specs can be seen below). These operates on the lower of the S-Band range at 2.0-2.3 GHz, with a downlink data rate (Tx) around 4 Mbps while the uplink data rate (Rx) is about 64 kbps. The payloads data rate was about 13.1 kbps and any housekeeping instructions related to propulsion and ADCS would only be about 10 kb in size which fit into the component's data specifications, this plus the fact that both transceiver and patch antenna had a TRL of 9 made this a safe choice for the satellite.[20][21]

4.2.2. Transeiver

Transceiver Data	
	SLink-PHY
Uplink Speed (Ground - Sat)	64 kbps
Downlink Speed (Sat – Ground)	4 Mbps
Power (Max)	13 W

Table 13: Transeiver Data

4.2.3. Antenna

Antenna Data	
	S Band Antenna
Style	Patch

Operation frequency	1.980-2.500 GHz
Outer dimensions	70 x 70 x 3.4 mm ³
Mass	49 grams
TRL	9

Table 14: Antenna Data

4.3. Results

From the STK scenario as described in the previous section the team was able to analyze the access times for each ground station location along with general information about access periods over the scenario. Analyzing the effects of weather and interference on access time revealed that the effects have minimal change the access periods and can be largely disregarded.

Data Rate	Time Collecting	File Size
13.2 kb/s	100	1320 kb (1.32 Mb)
	1000	13200 kb (13.2 Mb)
	5000	66000 kb (66 Mb)
	5656	74659 kb (74.7 Mb)

Table 15: File Size Per Data Collection Time

An estimation for file size can be made based on the given data rate found earlier (~13.2kb/s) and how long the scientific payloads spend collecting data. The team agreed on continuous data collection for an entire orbital period, shown on the table in bold, resulting in a file size of ~75 Mb. With a transmission rate of ~4 Mb/s files of these size can easily be transmitted in the access windows available, even allowing for limiting data transmissions to every other orbit if necessary.

4.4. WPI Ground Station Set-Up

Part of this project was devoted to continuing researching what would be required to set up a ground station at the WPI. In previous years they found that a handful suppliers who sold ground station kits. These kits included everything required to set up a station, which makes gathering all the individual components much easier as they are bundled together and are confirmed to be compatible with each other. Based on previous years recommendations more research was done into ISIS Full Ground Station Kit for VHF/UHF, which parts list are shown below:

Instrumentation Rack containing:

- VHF / UHF ground station transceiver
- S-band Receiver
- Rack mount PC with Local Ground Station (LGS) software
- Cavity filters to suppress UMTS interferences.
- Rotator Controller

Steerable Antenna System

- Azimuth and elevation rotators with speed upto 6° /sec
- Hot-dip galvanized steel mounting mast
- UHF and VHF Yagi antennas
- 2m dish with helix feed, LNA and cavity filters for S-band (2200 – 2290 MHz or 2400 – 2450 MHz)
- Lightning protection system
- 20m of cable between 19"rack and antenna included in price

Standard Software

- Satellite tracking software pre-installed
- Autonomous tracking with scheduler
- Debian/GNU LINUX operation system pre-installed

Compact setup

- The ground station equipment (except the antenna system) is fitted into a single 12-U 19” rack which allows the ground station to fit in almost any location.

Remote Operations

- It is possible to configure and control the ground station remotely through the internet. []

When they recommended this the price was around \$80,000 however the price has risen to around \$97,000 dollars. Due to this price hike the team is now recommending a different version of this kit which comes with all of the same equipment without the transmitter, this kit lowers the cost to ~\$75,000. While this removes some functionality from the ground station the majority of the transmission done by these mission types is downlinking data therefore the transmitter is not a vital part for this ground station. By buying this kit it would allow most if not all of the data to be transmitted at the WPI ground station limiting the dependency on other ground stations to just uplinking. Another benefit is the fact that this kit is not permanently limited to just receiving data, a transmitter can be bought separately and added to the station, making this kit a good starting point that still providing a large benefit to potential projects.

5. COMMAND AND DATA HANDLING

5.1. Overview

The command and data handling (C&DH) subsystem encompasses the brain of the satellite and has primary goals of: ensuring that the spacecraft has the computational capability for closed loop ADC and that the spacecraft has data capacity for science data. The primary components of C&DH subsystem are: on-board computer to manage the satellite functions and data storage systems.

The main functions that C&DH will manage are: issue instructions to propulsion system, issue instructions to ADC system, collect sensor and payload data, store sensor and payload data until transmission and transmit sensor and payload data when in range of ground station

5.2. Component Selection

5.2.1. Previous On-Board Computers

There have been several OBCs used in previous MQPs which are listed below with their corresponding year and whether they are still in production.

Year	OBC	Still in Production?
2011	MSP430x5xx	Yes
2012	Clyde Space Mission Interface Computer	No
2013	ADL LX8PC-AMD LX800	Yes
2018	Clyde Space 01-02928	No
2020	Clyde Space Kryten-M3	Yes

Table 16: Previous On-Board Computers

Of these OBCs which are still in production only the Clyde Space Kryten-M3 is up to date and with current hardware.

5.2.2. Chosen On-Board Computer

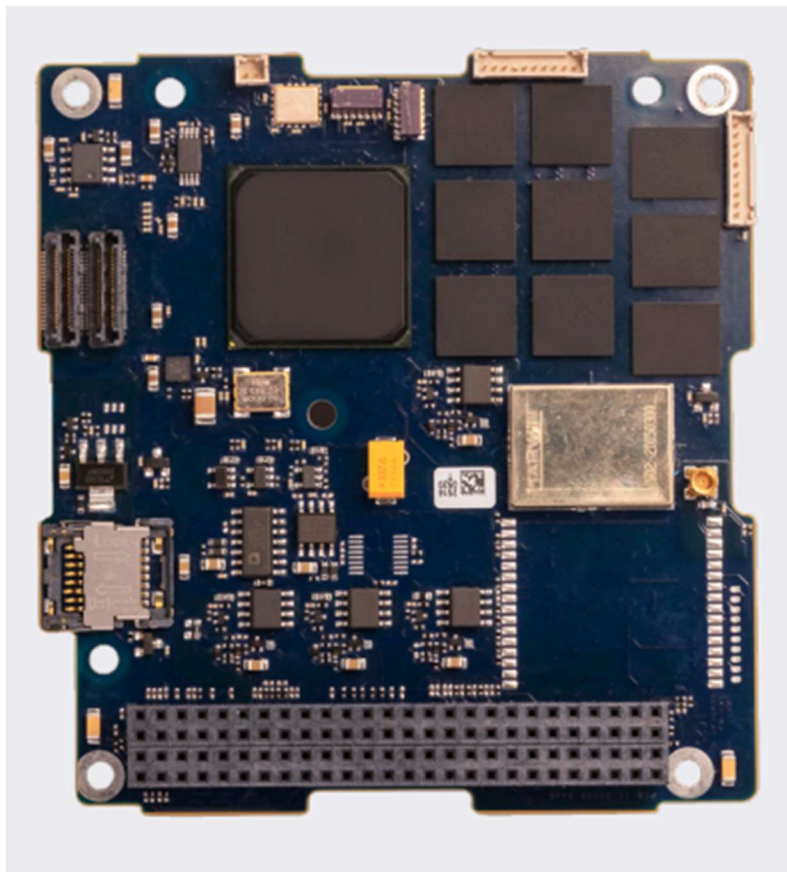


Figure 21: Kryten-M3

For the Appleton satellite we plan to use the Clyde Space Kryten-M3 Plus, this is due to its ease of use and meeting the necessary mission requirements; an easy-to-use operating system, an SSD port for additional data storage, and processing power capable of meeting the preliminary expected computational data needed. We plan to use the Kryten-M3 Plus rather than the standard model because it includes a GPS.

6. CONCLUSION AND RECOMMENDATIONS

The goal of this project was to design some of the primary subsystems for a 6U CubeSat for an ionospheric mission. Appleton's primary mission objective is to further the understanding of the ionosphere by analysing its composition, local properties, and providing data to investigate any present anomalies utilizing the NASA-designed miniature Ion Neutral Mass Spectrometer (mini-INMS) and Gridded Retarding Ion Drift Sensor (GRIDS). This report detailed the design of the Payload, Attitude Determination and Control, Telemetry and Communications, and Command and Data Handling subsystems of the Appleton CubeSat design, with the other subsystems covered in separate reports.

The goal of Appleton's ADCS design was to provide functional detumble and maintenance via a closed-loop control system and deterministic algorithms. The Telemetry and Communications subsystem was required to provide ample access time for all needed data transfers. The Command and Data Handling subsystem was needed to provide sufficient computing power to run the on-board control systems required by the ADCS.

Considering the mission constraints and requirements, this segment of Appleton's mission design would require further simulation and testing before manufacture and launch readiness. Specifically, ADCS requires further simulation and testing to be considered flight ready. In future research, controllers must be fed with accurate model inputs and iteratively tested for optimal gain to achieve proper detumble and maintenance requirements. Future projects can work to better integrate the STK dynamics modelling with control systems design through Simulink. Further research into accurate sensor simulation in STK models would also be beneficial to robust system design. Apart from the technical gaps remaining in the ADCS,

Appleton's remaining subsystem designs are prepared to meet mission requirements. While further research and design are still needed in the areas highlighted above, this project has constructed a foundation for further design of related subsystems onboard CubeSat science missions.

REFERENCES

- [1] J. Blandino, N. Martinez-Baquero, N. Paschalidis, N. Gatsonis and M. Demetriou, "Feasibility for Orbital Life Extension of a CubeSat in the Lower Thermosphere," *Journal of Spacecraft and Rockets*, vol. 53, no. 5, 2016.
- [2] J. Klenzing, R. L. Davidson, G. D. Earle, A. J. Halford, S. L. Jones, C. R. Martinis, N. Paschalidis, R. F. Pfaff, J. M. Smith and K. A. Zawdie, "petitSat -A 6U CubeSat to examine the link between MSTIDS and ionospheric plasma density enhancements," in *AGU 100 Advanced Earth and Space Science Fall Meeting*, San Francisco, California, 2019.
- [3] M. Rodriguez, N. Paschalidis, S. Jones, E. Sittler, P. Uribe, D. Chornay and T. Cameron, "Miniaturized Ion and Neutral Mass Spectrometer for CubeSat Atmospheric Measurements," NASA Goddard Space Flight Center, Greenbelt, Maryland, 2016.
- [4] *Rev. Sci. Instrum.* 91, 064502 (2020); <https://doi.org/10.1063/1.5140470> Submitted: 27 November 2019. Accepted: 20 May 2020. Published Online: 17 June 2020.
- [5] M. Hatfield, "Dellingr: The Little CubeSat That Could," NASA, 23 October 2018. [Online]. Available: <https://www.nasa.gov/feature/goddard/2018/dellingr-the-little-cubesat-thatcould>. [Accessed 15 October 2021].
- [6] L. Keesey, "NASA Team Pursues Blobs and Bubbles with New PetitSat Mission" NASA, 09 May 2017. [Online]. Available: <https://www.nasa.gov/feature/goddard/2017/nasa-team-pursues-blobs-and-bubbles-with-new-petitsat-mission> [Accessed 15 October 2021].
- [7] Crassidis, J.L., and Markley, F.L., *Fundamentals of Spacecraft Attitude Determination and Control*, Springer, New York, 2014, Chaps. 8, 11.
- [8] Wertz, J.R., and Larson, W.J., *Space Mission Analysis and Design*, 3rd ed., Kluwer Academic, Boston, 1999, Chaps. 8, 11.
- [9] Avanzini, G., and Fabrizio, G., "Magnetic Detumbling of a Rigid Spacecraft," *Journal of Guidance, Control, and Dynamics*, Vol. 35, No. 4, July-August, 2012
- [10] Gatsonis, N.A., Lu, Y., Blandino, J., Demetriou, M.A., and Paschalidis, N., "Micropulsed Plasma Thrusters for Attitude Control of a Low-Earth-Orbiting CubeSat," *Journal of Spacecraft and Rockets*, Vol. 53, Issue 1, 2016
- [11] Hales, J.H., and Pedersen, M., "Two-Axis MOEMS Sun Sensor for Pico Satellites," 16th Annual AIAA/USU Conference on Small Satellites, 2002
- [12] D. Hyun Ko , S. Laudage, M. Murphy, D. Pelgrift and S. Young, "Design and Analysis of the Sphinx-NG CubeSat," Worcester Polytechnic Institute, Worcester, 2017

- [13] N. Bograd, G. Jacobson, P. Kroyack, C. Lopez and J. Peters, "Design and Analysis for CubeSat Missions," Worcester Polytechnic Institute, Worcester, 2018
- [14] R. Galliath, O. Hasson, A. Montero, C. Renfro, D. Resmini, "Design and Analysis of a CubeSat," Worcester Polytechnic Institute, Worcester, 2020
- [15] A. Brown, W. Cooley, A. Klenk, S. Messey, J. Meleti, A. Robatzek, M. St Jean, "Design of a NanoSat for an Ionospheric Mission," Worcester Polytechnic Insitute, Worcester, Massachusetts, 2021
- [16] NASA, "CubeSat101 Basic Concepts and Processes for First-Time CubeSat Developers," NASA, 2017.
- [17] Amazon Web Service, "AWS Ground Station" 2020. [Online]. Available: <https://aws.amazon.com/ground-station/> [Accessed 10 2021]
- [18] Amazon Web Service, "AWS Ground Station February 2020," 2020. [Online]. Available: https://esto.nasa.gov/wp-content/uploads/2020/03/AWS-FCD_GroundStation_Feb2020-NOS.pdf [Accessed 10 2021].
- [19] NASA, ""Near Earth Network (NEN) Users' Guide," March 14, 2019.[Online]. Available: https://explorers.larc.nasa.gov/2019APSMEX/SMEX/pdf_files/453-UG-002905.pdf [Accessed December 2021].
- [20] IQspacecom, "SLink-PHY." 2019 [Online] Available: <https://www.iq-spacecom.com/products/slink-phy> [Accessed 10 2021]
- [21] IQspacecom, "Antenna S-band." 2019 [Online] Available: <https://www.iq-spacecom.com/products/antenna-s-band> [Accessed 10 2021]
- [22] Wahba, G. A Least Squares Estimate of Satellite Attitude." SIAM Review, 7(3), p. 409

APPENDIX A: KRYTEN M3 TECH SHEET

TECHNICAL SPECIFICATIONS

General	
Design Life	5 years in LEO
Processor	Smart Fusion 2 SoC including an ARM Cortex-M3 processor delivering 62.5 DMIPS
Processor Clock	50 MHz
SCET	Real time counter (w/40mins. Backup Power)
MRAM	8 MB
Operating Temperature Range	-40°C to +80°C
Boot Image Storage	256 kB eNVM + 8MB MRAM
Radiation (TID)	20 kRAD
Typical Energy Usage	6.4 mJ/DM
GPS (PLUS model only)	<10m RMS position accuracy <1m/s RMS velocity accuracy

Interfaces		
I2C		2
SPI	7 Chip Select Lines	1
UART	3.3 V Logic	8
RS422 1	(can be used as 2xRS485)	1
CAN		1
DTMF		1
	JTAG w/ETM Support + 1 Serial	
Debugging	Debug	1
LVDS	20x Lines, Expansion	1
QSPI	[2x LVDS, 1x 3V3 Logic]	3
GPIO	3.3 V Logic	17

* Not all interfaces available simultaneously

Size, Weight & Power	
Nominal Power Consumption	400 mW (typ), 1 W max
Mass	61.9 g
Length	95.89 mm
Width	90.17 mm
Height*	5.51 mm

* Height from top PCB to lowest component



To make an enquiry, request a quotation or learn about AAC Clyde Space's other products and services, please contact: enquiries@aac-clydespace.com



#SPACEISAWESOME

www.aac-clyde.space

Copyright AAC Clyde Space 2021. All rights reserved.
All information subject to change. Release date 28 July 2020.